AWARD NUMBER: W81XWH-11-1-0752

TITLE: Mechanism and therapy for the shared susceptibility to migraine and epilepsy after traumatic brain injury (TBI).

PRINCIPAL INVESTIGATOR: K.C. Brennan M.D.

CONTRACTING ORGANIZATION: Univeristy of Utah
Salt Lake City, UT 84112

REPORT DATE: December 2015

TYPE OF REPORT: Final

PREPARED FOR: U.S. Army Medical Research and Materiel Command
Fort Detrick, Maryland 21702-5012

REPORT DOCUMENTATION PAGE		Form Approved OMB No. 0704-0188
1. REPORT DATE December 2015	**2. REPORT TYPE** Final	**3. DATES COVERED** 09/30/2011- 09/29/2015
4. TITLE AND SUBTITLE Mechanism and therapy for the shared susceptibility to migraine and epilepsy after traumatic brain injury.		**5a. CONTRACT NUMBER** **5b. GRANT NUMBER** W81XWH-11-1-0752
6. AUTHOR(S) KC Brennan, Ed Dudek, Jeremy Theriot, Punam Sawant, Dan Kaufmann. E-Mail: k.c.brennan@hsc.utah.edu		**5d. PROJECT NUMBER** PR100060 **5e. TASK NUMBER** **5f. WORK UNIT NUMBER**
7. PERFORMING ORGANIZATION NAME(S) AND ADDRESS(ES) University of Utah 383 Colorow Drive, Room 364 Salt Lake City UT 84108		**8. PERFORMING ORGANIZATION REPORT NUMBER**
9. SPONSORING / MONITORING AGENCY NAME(S) AND ADDRESS(ES) U.S. Army Medical Research and Materiel Command Fort Detrick, Maryland 21702-5012		**10. SPONSOR/MONITOR'S ACRONYM(S)** **11. SPONSOR/MONITOR'S REPORT NUMBER(S)**

12. DISTRIBUTION / AVAILABILITY STATEMENT

Approved for Public Release; Distribution Unlimited

13. SUPPLEMENTARY NOTES

14. ABSTRACT

Our proposal has examined the natural history and mechanisms of increased brain excitability leading to migraine and epilepsy after traumatic brain injury (TBI). In order to pursue our work, we have pioneered or significantly advanced new techniques for the study of TBI, including continuous remote telemetry, *in vivo* whole cell recording, and two-photon imaging with genetically encoded calcium indicators. We have generated multiple reportable outcomes, providing experimental evidence that: 1. TBI causes seizures; 2. TBI increases neuronal excitability, an effect that is enhanced in 'migraine' mutant mice; 3. TBI is universally associated with spreading depolarizations that are also involved in migraine; 4. sensory cortex is more susceptible to spreading depolarizations, consistent with prominent sensory and pain features after TBI; 5. the effects of TBI are amplified by female sex as well as migraine genotype, consistent with what is observed in the clinic. We have published four manuscripts (in Science Translational Medicine, Stroke, Journal of Neurophysiology, and Cephalalgia); two more are pending publication; and four more manuscripts are in preparation. This work also continues in CDMRP PR130373.

15. SUBJECT TERMS

Traumatic brain injury, cortical spreading depression, seizure, post-traumatic headache, post-traumatic epilepsy, migraine, epilepsy.

16. SECURITY CLASSIFICATION OF:			**17. LIMITATION OF ABSTRACT**	**18. NUMBER OF PAGES**	**19a. NAME OF RESPONSIBLE PERSON** USAMRMC
a. REPORT Unclassified	**b. ABSTRACT** Unclassified	**c. THIS PAGE** Unclassified	Unclassified	62	**19b. TELEPHONE NUMBER** *(include area code)*

Standard Form 298 (Rev. 8-98)

Table of Contents

1. INTRODUCTION

Despite great improvements in medical care, traumatic brain injury (TBI) remains the leading cause of death in those under 40 years of age[1,2], in both civilian and military populations. Moreover, as protective strategies and acute treatment have improved, TBI survivors are often profoundly affected by the long-term consequences of injury. These long-term consequences include two disorders of altered brain excitability: chronic headache (usually chronic migraine) and epilepsy. Our proposal examines the links between TBI and these two conditions, which themselves are closely related[3] and can occur in the same patient after injury. Our underlying hypothesis is that the shared susceptibility to migraine and epilepsy after TBI is due to a long-term increase in cortical excitability induced by brain trauma.

2. KEY WORDS

Traumatic brain injury, migraine, epilepsy, cortical spreading depression, controlled cortical impact

3. OVERALL PROJECT SUMMARY

Specific Aim 1
Determine whether TBI causes a self-perpetuating increase in excitability that sets the stage for epilepsy or chronic migraine

Major Task 1. Acute/subacute experiments after controlled cortical impact (CCI) TBI (Brennan, Dudek, Months 1-48)

Subtask 1:
Perform CCI, implant monitoring device, and monitor for acute/subacute effects of TBI (7 days after injury)

Methods:

Dudek Lab CCI Procedure.

Male, C57B1/6 mice (n=30) were anesthetized with 2-4% isoflurane and pretreated with atropine (2 mg/kg), and penicillin (0.2 mL, SC, 300,000 IU). The surgical site was shaved, prepped with betadine scrub and solution and isolated with sterile surgical towels. For the CCI procedure, once the mouse was secured in the stereotaxic unit, a rectal probe was inserted and a rectal temperature of 37 ± 0.5 °C was maintained with a temperature-controlled heating pad. Next, a mid-sagittal skin incision was made from the occipital notch to the forehead. A dental drill was used to perform a 3-mm craniotomy, using bregma, and coronal, lambdoidal, and interparietal sutures as landmarks. A microprobe (Physiotemp) was inserted through a burr hole into the left frontal cortex to monitor brain temperature, which was maintained at 37 ± 0.5 °C by adjusting the warming blanket and warming lights. For the injury 1-mm metal impactor tip was pneumatically driven at a velocity of 4.0 m/s, depth of penetration 1.0 mm and duration of 100 ms to induce the traumatic brain injury.

For the EEG recordings 2 holes were drilled into the skull for the support screws and the two wire EEG electrodes placed on the dura over the CCI-injury site. The entire electrode unit was secured to the skull with dental cement. The skin surrounding the electrode base was sutured shut with non-dissolvable suture. Bupivacaine (7.5mg/ml, SC) was applied to all surgical sites. Age-matched sham craniotomies served as controls. Shams underwent anesthesia and preparative surgery but no CCI.

EEG analysis

Thus far, we have manually analyzed data of video-EEG recordings. Given the labor intensive manner of manually analyzing the video-EEG data (Figure 1), we have developed a semi-automated seizure detection program (as shown in Figure 2). Currently, we are re-analyzing our EEG data from sham and CCI animals, using this automated analysis program.

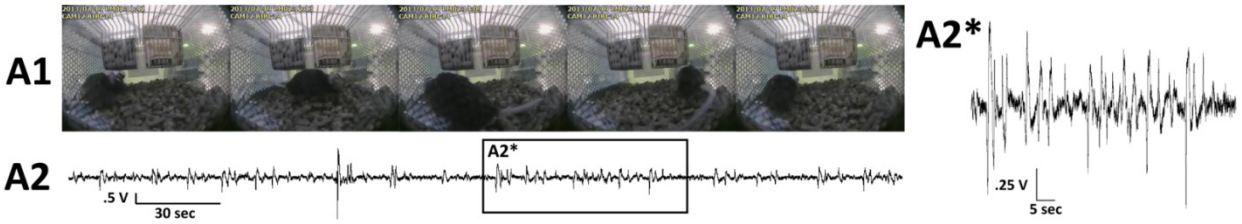

Fig. A1,A2: Ambulatory behavior not detected by routine with video. A2*) Higher amplitude spiking from normal waveforms described by VR

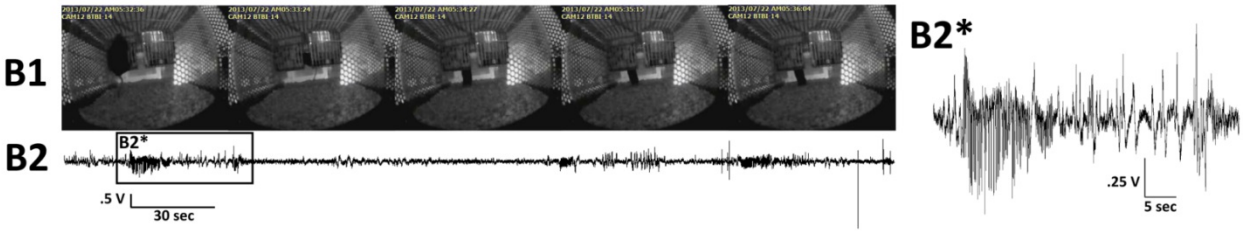

Fig. B1,B2: Climbing behavior not detected by routine with video. B2*) Area of interest- regular patterns of spiking described by VR

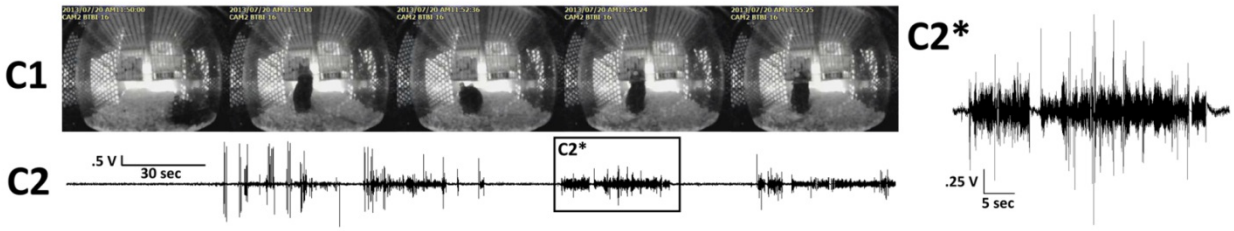

Fig. C1,C2: Eating behavior detected by routine and confirmed by post-hoc VR. C2*) Dense spiking clusters described by VR

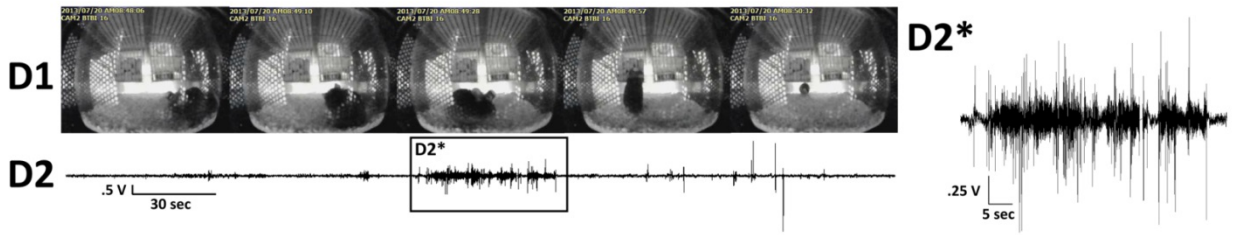

Fig.D1,D2: Grooming behavior partially detected by routine. D2*) High amplitude spiking with dense high-frequency patches described by VR

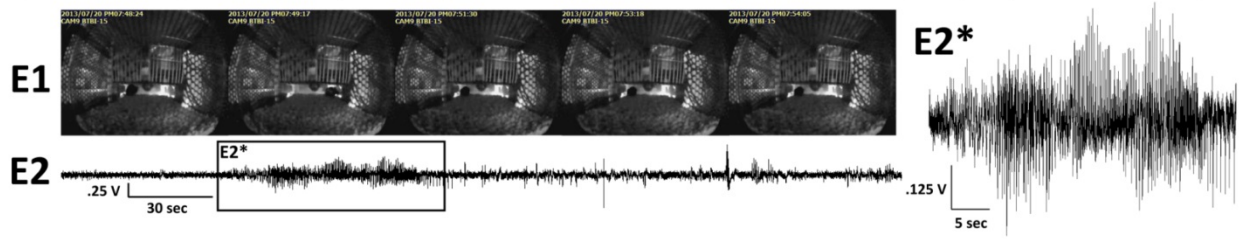

Fig. E1,E2: P3 seizure detected by routine and confirmed by post-hoc VR with video confirmation. E2*) Likely seizure as described by VR

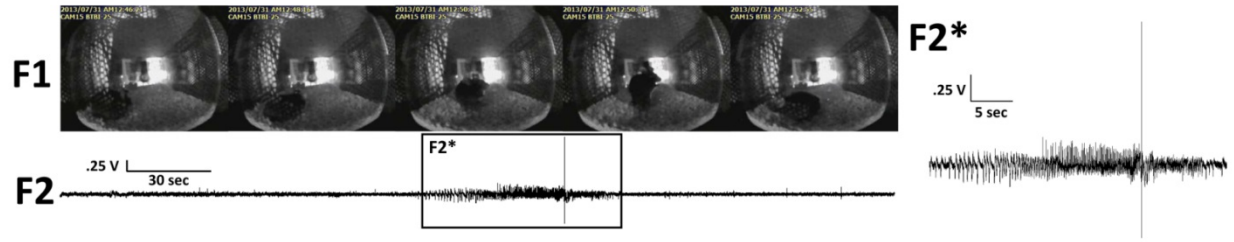

Fig. F1,F2: P5 seizure detected halfway after start by routine with post-hoc video confirmation. F2*) Likely seizure as described by VR

Figure 1: We compared visual review (VR) with the routine's output for detecting EEG events of interest with the current algorithm parameters. Example screen shots are shown of visual review conducted with AcqKnowledge (top) compared to the routine GUI output for post-hoc visual review (bottom). Events with slow spiking, such as ambulation (A2*) were not detected due to the spike number requirement parameter of the routine. Events with substantial spiking but little autocorrelation, such as climbing (B2*) were also not detected by the autocorrelation-based routine. The repetitive nature of grooming and eating were detected (C2* and D2*), with some high-voltage spiking caused by the wireless telemetry system (Epoch) touching the metal food dispenser and stopping the system's ability to transmit to the receiver antenna, which results in a temporary loss of signal. P3 and P5 level seizures (E2*,F2*), as defined by "probable seizure" (P) of magnitude (#) based on a modified Racine scale, were detected by the algorithm, due to high autocorrelation and significantly high number of spiking events. The partial detection of the P5 seizure was due to slow-wave spiking at seizure onset. Most seizure events and events of interest were identified, with many false positives and some events not matching the routine's set parameters.

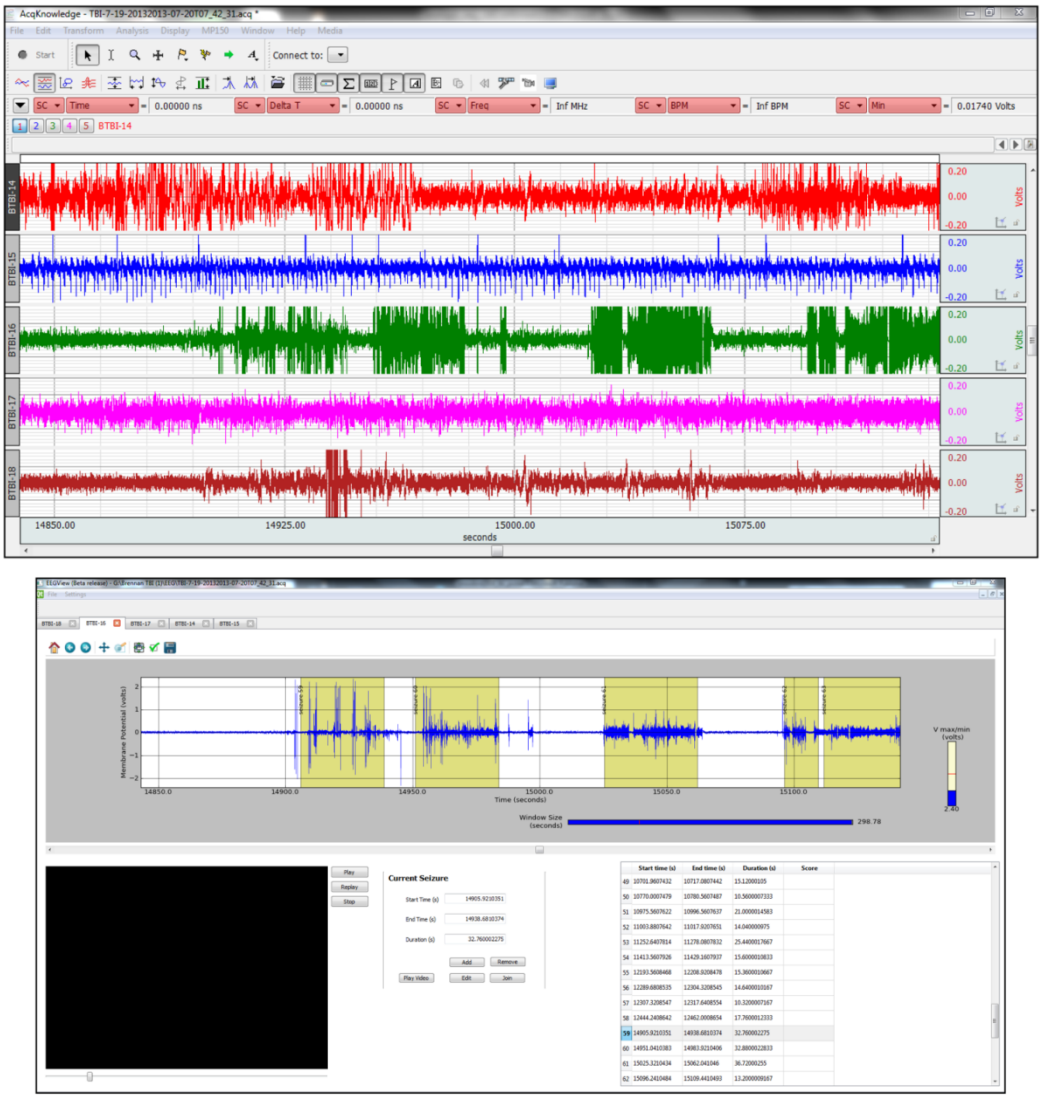

Figure 2: Summary of the validation process for the semi-automated seizure detection program.

Results

To continue testing the hypothesis that acute seizures following a traumatic brain injury may be a predisposing factor for the development of PTE, we subjected mice (n=13) to a moderately severe CCI injury. Immediately after the impact, the mice were implanted with a wireless EEG telemetry device. To serve as a control, sham-operated mice (n=11) underwent the same surgical procedures but were not injured. Video-EEG data were collected continuously for 90 days.

Mortality & lost recordings.

For sham group, we started with n = 11 animals but we lost 2 animals because one died and another animal lost its recording. We started our experimental (CCI) group with n = 13 animals but we lost 5 animals (3 animals died and 2 animals lost their recording) within 1-5 days after CCI.

Early seizures (0-7 days post-sham/CCI)

Two of 10 sham-treated animals had early seizures (20% of animals). One animal had one seizure/day, and another animal had 3 seizures/day.

Six of 12 CCI-animals showed acute seizures (50% of animals; 120 $\pm$ 30 s). These animals showed 1-8 seizures/day (range). Nine hours after injury, one mouse developed status epilepticus (Figure 2) which continued for 3 days resulting in the animal's death.

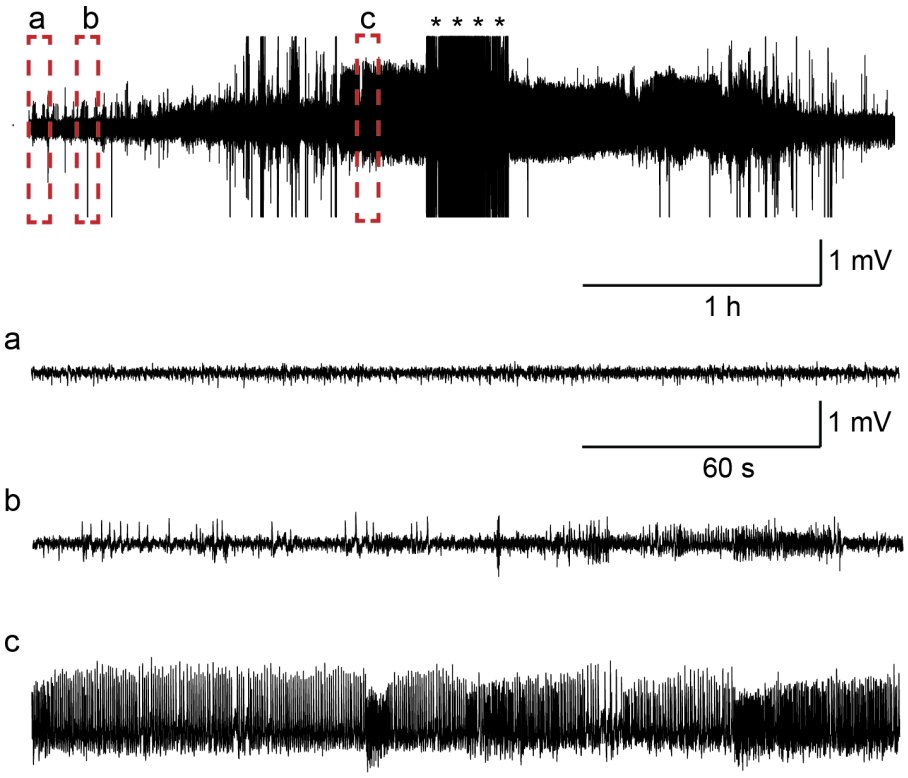

Figure 3: Electrographic recording of a CCI-injured mouse in status epilepticus. Upper trace is an EEG recording of 4 h of status epilepticus while the lower traces represent portions of the EEG within the

dashed boxes at an expanded timescale. The recordings below demonstrate the baseline EEG (a), an individual seizure (b) and the continuous spiking evident of status epilepticus (c). * represents movement artifact from the seizure motor activity.

Late seizures (i.e., epilepsy post-sham/CCI)

Two of nine animals from the control group showed spontaneous seizures in this chronic period (22 % of animals). One animal showed seizures at 30 days (one seizure/day) however, this animal did not show any seizures immediately after sham treatment. Another animal showed seizures at 60 days post-sham treated animals (30 $\pm$ 3 s; 3 seizures/day).

One animal (one of 8 animals) started having seizures 7 days after CCI injury (13% of animals; 58 $\pm$ 4 s; Figure 3). For the CCI-injured mouse, the seizure frequency was possible 7-9 seizures/day).

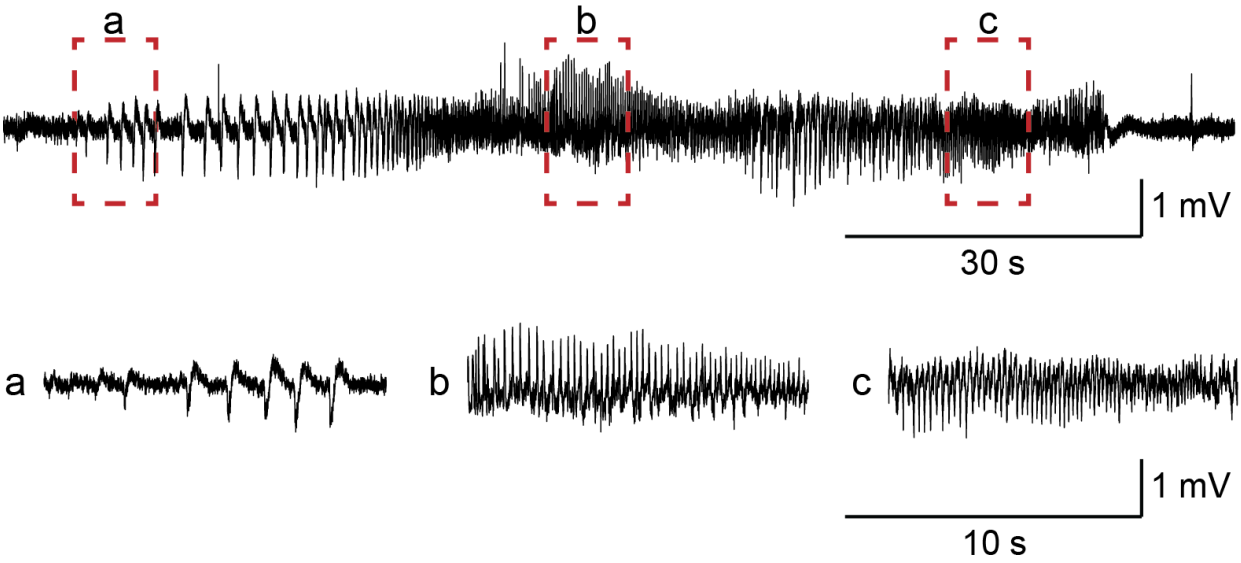

Figure 4: A spontaneous recurrent seizure in a CCI-injured mouse. An example of an electrographic seizure recorded from a CCI-injured mouse 28 days after the injury. The EEG traces below were selected from the areas highlighted by the dashed boxes. Illustrated in an expanded time scale is the spiking pattern from the beginning (a) middle (b) and end (c) of the seizure.

Although we have successfully recorded spontaneous seizures from CCI-injured mice for 90 days, some concerns exist. First, more analysis is required to determine the fraction of animals that develop epilepsy, the temporal pattern of their seizures, and their maximal seizure frequency. The second is that the incidence of seizures in the CCI-injured mice was low (46%). The fraction of epileptic animals may be higher with further analysis. In order to test the effects of memantine on the development of post-traumatic epilepsy, however we may have to increase the number of animals in the study. As is evident clinically, the time from the injury to the development of late spontaneous recurrent seizures can be lengthy and variable. In order to maximize our ability to detect late seizures, we can increase the duration of EEG recordings from 90 to 120 days.

The third caveat is that early or subacute seizures were recorded from 20% of the sham-operated controls (Figure 5). Seizure/epileptiform activity in sham-operated controls has been reported by others[4]. Clinically, a risk factor for developing epilepsy is having undergone a craniotomy. Craniotomies themselves can produce neuronal damage [5]. In the future, we will include a control group without craniotomy.

The fourth caveat is that the mortality in the CCI-injured mice was 46%. The majority of the mortality occurs within 1 week following the injury. Although this mortality rate is similar to what has been reported in other TBI studies with moderate-severe injury, we can work to minimize this, by either altering the depth of the injury or adjusting the location of the impact.

The fifth caveat is that we lost EEG recordings over time in both the sham-operated and CCI-injured mice. A loss of the EEG recording (33% in the CCI-injured group) resulted from either a loss of the recording electrode from the animal's head or a dead battery in the unit. To minimize the loss of recording electrodes, we will secure the unit to the animal's head with an additional support screw. Although the animals are implanted with units containing a 6-month battery life, the units can fail prematurely. We are working with the supplier to insure that the units will have the appropriate battery life to complete the study.

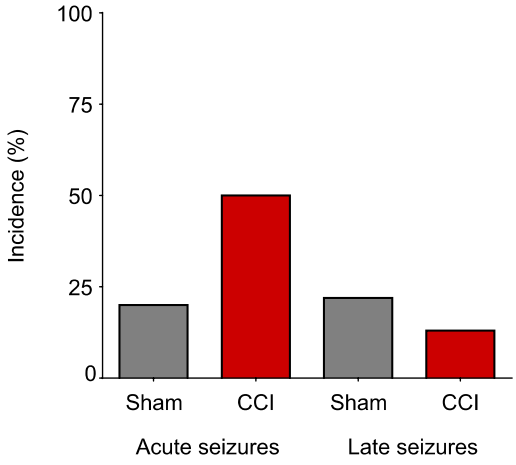

Figure 5: Bar graph showing the incidence of seizures in both the sham-operated controls and CCI-injured mice during acute and chronic periods.

Despite the caveats, this is the first continuous longitudinal study of the incidence of post-traumatic seizures. We know of no other study that has performed continuous monitoring to even a fraction of the time we observed. We conclusively show that TBI generates seizures, and we are making the argument in our manuscript that our sham treatment really is not a sham but a milder form of brain injury. Both are important reportable outcomes for TBI and epilepsy.

Seizures and possible cortical spreading depression (CSD) after CCI TBI.

In a separately funded study we have been recording in rats after CCI. These animals are shown because they demonstrate a long-lasting EEG suppression that resembles what would be seen in an alternating current (AC) recording of cortical spreading depression. In this study, experimental animals (n=5) underwent similar CCI procedures to mice, scaled up for rat, while control animals (n=5) underwent a craniotomy and EEG electrode implantation only. Video-EEG data was recorded within 30 min of the injury and for 3-7 days post CCI-injury with a

tether-based EEG recording setup. In the majority of the CCI-injured rats, the background EEG signal was suppressed for several hours (see Figure 6c). This suppression in background EEG may be caused by spreading depression. Subacute seizures were observed in 40% of rats (see Figure 6a,b). We are currently analyzing our mouse data to detect this phenotype. Preliminarily, we do not detect it as robustly as in rat; one difference in preparation that may be relevant is that rats were recorded with a tethered system which has a high pass cutoff (low frequency range) broader than the wireless telemetry devices we are using in mice.

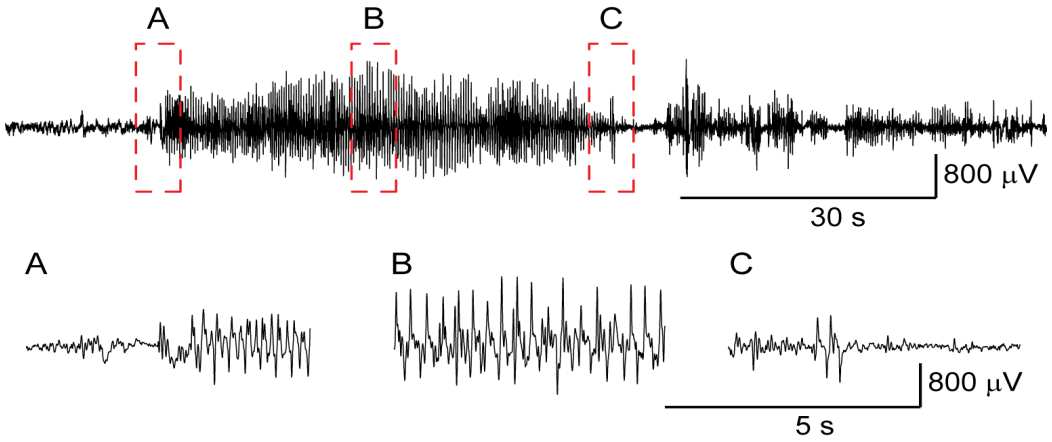

Figure 6: An example of an electrographic seizure recorded from a CCI-treated rat recorded 3 days post CCI injury. The traces below are expansions of the EEG located in the red dashed boxes. Temporal progression of the beginning (A) middle (B) and end of the seizure (C).

Subtask 2. Perform CCI, thresholding for seizure, cortical spreading depression.

CCI universally generates cortical spreading depression

We used Leica Impact One steroteaxic impactor [6], 4 m/s velocity, 100 ms dwell time, 1 mm impact depth, with a 1 mm diameter flat tipped impactor for all experiments in the Brennan lab. With these parameters, we observed cortical spreading depression (CSD) with every induction (n>200 animals total). This shows conclusively that CSD is an obligate component of traumatic brain injury, and justifies its study as a TBI mechanism.

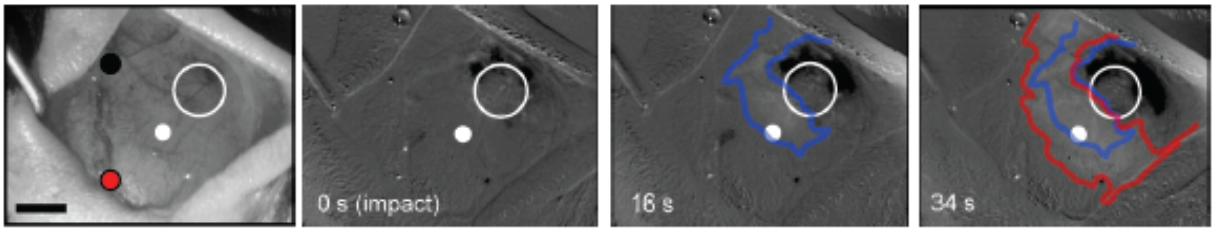

Figure 7: Controlled cortical impact TBI. Typical CCI preparation. Shaved sterilized skin is retracted, 2mm craniotomy is seen to the right of top center, under a saline meniscus. Impactor tip is to the right of the craniotomy. Difference images, labeled with time from impact, show expanding increase in light reflectance, consistent with cortical spreading depression as reported by our lab[7–9] and others[10]. This was seen with every imaged CCI induction (n>50) and was readily observable with the naked eye by experienced observes (n>200).

STAT3 conditional knockout (STAT3-CKO) enhance our mechanistic understanding of TBI effects.

Our collaborator Dr. Michael Sofroniew was originally going to provide us with mGFAP-YFP mice, which express yellow fluorescent protein in astrocytes, allowing for specific imaging. These mice have unfortunately been inconsistent in their gene expression. As an alternative Dr. Sofroniew provided us with STAT3-CKO mice. These animals also allow for identification of astrocytes, but have the additional benefit that they allow testing of a signal pathway involved in astrocyte reactivity after TBI. STAT3-CKO mice have selective inactivation of STAT3 in astrocytes through the mGFAP promoter and show disrupted glial scarring and attenuated astrogliosis surrounding spinal cord injury [11]. STAT3 is ubiquitous member of the Jak-STAT signaling family, responsible for the signaling of many cytokines and growth factors [12]. STAT3 is expressed by most cell types in the CNS, and is up- regulated following traumatic brain injury in rodents [13]. The time course of phosphorlyated-STAT3 (activated STAT3) was shown to begin shortly after TBI gaining peak levels around 24 hours, and levels returning to baseline at 7-days, with phosphorylated-STAT3 shown to colocalize predominantly with astrocytes [13]. This tool significantly amplifies the mechanistic power of our proposal. However the cost of additional animals or experiments (specifically those involving STAT3 transgenic animals; wild-type animal experiments are as we proposed initially) has not been borne by CDMRP as STAT3 mice were not in the original proposal.

CCI does not affect induced CSD susceptibility in WT or STAT3-CKO animals.

CSD susceptibility was measured 48 hours and 7 days following injury. The CSD susceptibility procedure consists of re-opening the now fully healed suture in the anesthetized animal to expose the top of the skull. Carefully placed burr holes (being very cautious not to disrupt the dura matter) are placed in both the injured (ipsilateral) and uninjured (contralateral) hemispheres. Microcapillary tips are placed inside the burr holes producing a constant flow (~3.2 μL/min) of 0.9% saline to start. The animal's vital signs and temperature are monitored throughout the surgery. A thin layer of silicone oil is applied to the top of the skull to enhance visibility through the skull. Approximately 15 minutes of images taken with a CCD camera using 535 nm LED illumination (a wavelength that increases hemoglobin contrast) are acquired before the solution perfusing the burrhole is switched to 1 M KCl to induce CSD events. Figure 8 displays the preparation. Difference images highlight the reflectance changes associated with CSD. Regions of interest placed in both hemispheres show the OIS fluctuations from each event, example shown in traces of Figure 8. The number of CSD events in both injured and uninjured hemispheres is recorded for 1 hr following the first CSD event. Figure 9 shows the results (n=10 animals/group). Interestingly, we see no significant difference in CSD number, ipsilateral or contralateral to CCI, in sham vs. CCI treated animals or in STAT3 transgenic animals vs. controls, at 48 hours and 7 days after CCI. Given the necessity of live tissue for the propagation of CSD [10] and the loss of tissue in injured cortex, we suspect there is a relative increase in the susceptibility of injured cortex. Follow-up experiments with either electrical stimulation or thresholded alterations in $[K^+]$ in perfusing solution could help test this hypothesis [7,14]. The lack of an effect of STAT3 genotype on CSD number suggests that astrocyte reactivity does not contribute to CSD susceptibility, at least in this preparation. However here again follow-up

experiments with electrical or thresholded KCl stimulation might uncover more subtle differences.

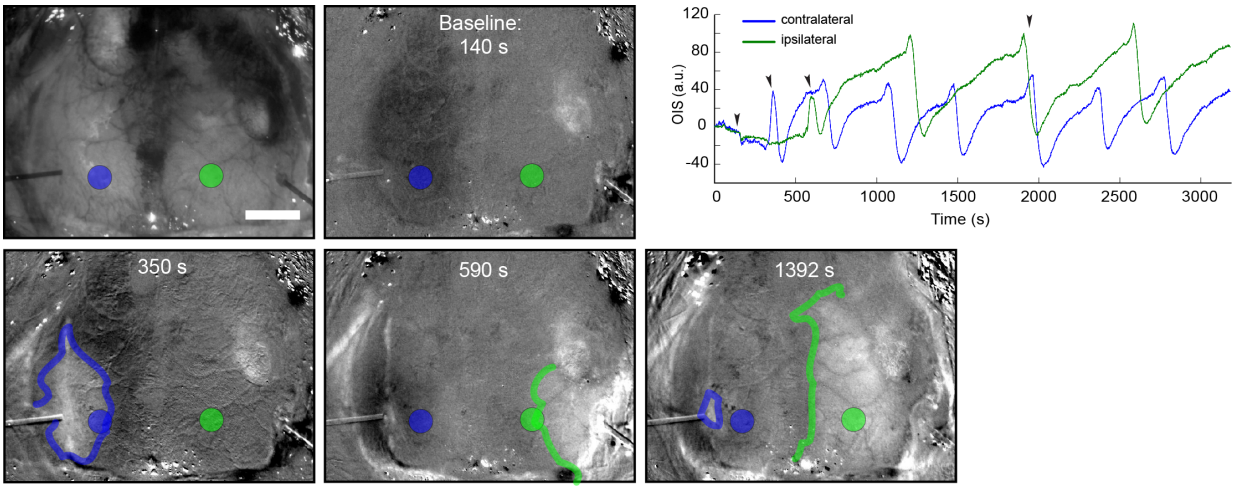

Figure 8: One week following TBI injury or Sham injury both WT (n=5 injury; n=2 sham) and KO (n=6 injury; n=3 sham) mice were subjected to dual hemisphere. CSD frequency measurement in response to 1 M KCl. Reference image followed by difference images highlight the reflectance changes associated with the CSD. Interestingly no differences were observed in CSD frequency 1 week post TBI.

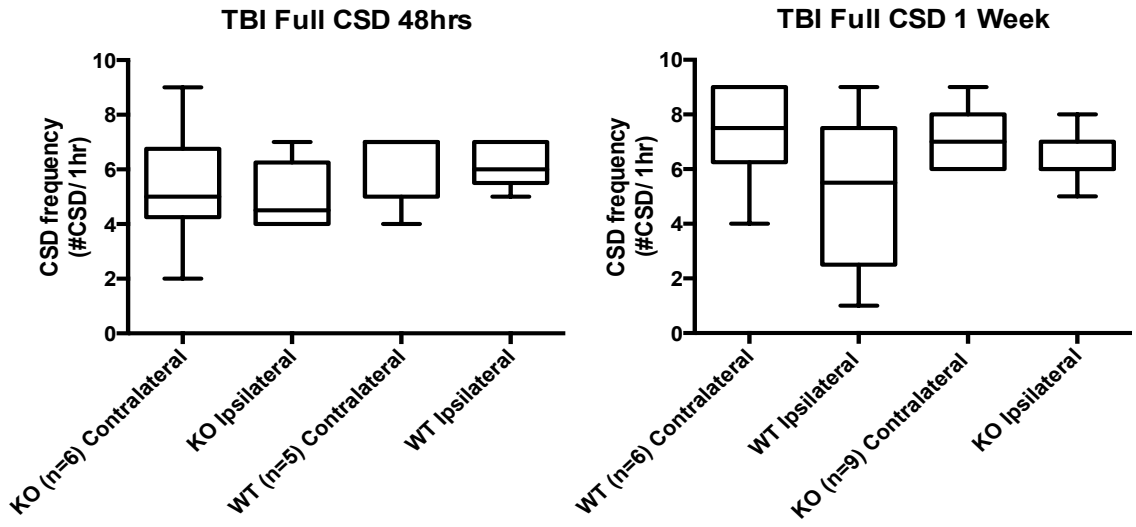

Figure 9: Pronounced astrogliosis and increased GFAP expression was observed in the injured cortex of both WT and KO mice, however, KO mice had significantly less GFAP expression level than WT animals in the injured cortex consistent with previous findings using the Stat3 KO mouse.

Subtask 3. Perform two-photon experiments 72 hours after CCI.

Calcium imaging with Oregon green BAPTA1-AM.

We initially performed calcium imaging of cortical cell populations by bolus loading of Oregon green BAPTA1-AM (OGB). Oregon-Green 488 BAPTA-1 AM is prepared at a concentration of

1 mM. We use a 20% solution of Pluronic F-127 in DMSO and we dissolve 50µg of OGB in it to a concentration of 10 mM. Then this solution is further diluted (to a 1mM solution) in a HEPES aCSF (150mM NaCl, 2.5mM KCl, 10mM Hepes, with a pH of 7.4). The calcium indicator is loaded in a glass pipette and bolus loaded in the cortex at a depth of 200µm (typically using a pressure of 10 PSI for 1 minute) [15]. Imaging is started after an hour of the pressure injections. An example of calcium imaging during CSD event is shown in Figure 10. However while is has been useful in uninjured animals, OGB use after TBI has proved problematic; thus we have switched to genetically encoded calcium indicators.

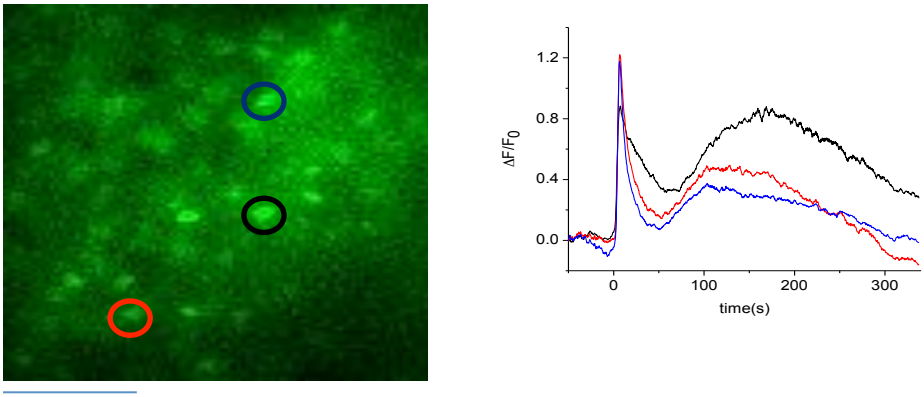

Figure 10: OGB1 AM loading of a cell population in layer 2/3 of somatosensory cortex (OGB1 selectively labels neurons, but some astrocyte fluorescence is also possible). The fluorescence changes corresponding to the occurrence to a CSD at t=0s in the areas depicted by colored circles are shown in the plot in the right side. The bar indicates 50 µm.

Imaging with genetically encoded calcium indicators (GECI).

The alternative to dye loading is to use GECI [16,17]. We use GCaMP5 or 6 delivered by viral vector injections. The use of AAV2/1.hSynap.GCaMP5G.WPRE.SV40 reveals neuronal specific population calcium activity in the relevant area of the cortex, because the expression is driven by the neuron-specific Synapsin promoter (Figure 11). For this procedure, the animal is anesthetized with isoflurane (5% for induction and 1.5% for the rest of the procedure) and put in the stereotactic apparatus for the correct identification of the region of interest. A small craniotomy is performed, and a small volume (~1 µL) of the virus suspension is loaded in a glass pipette and pressure injected. The craniotomy is sealed with silicone elastomer and the skin reapposed with vetbond. The animal is administered antibiotics and analgesics and recovered for 2 or 3 weeks to allow for a sufficient expression of GCaMP. After this the animal is prepared for imaging.

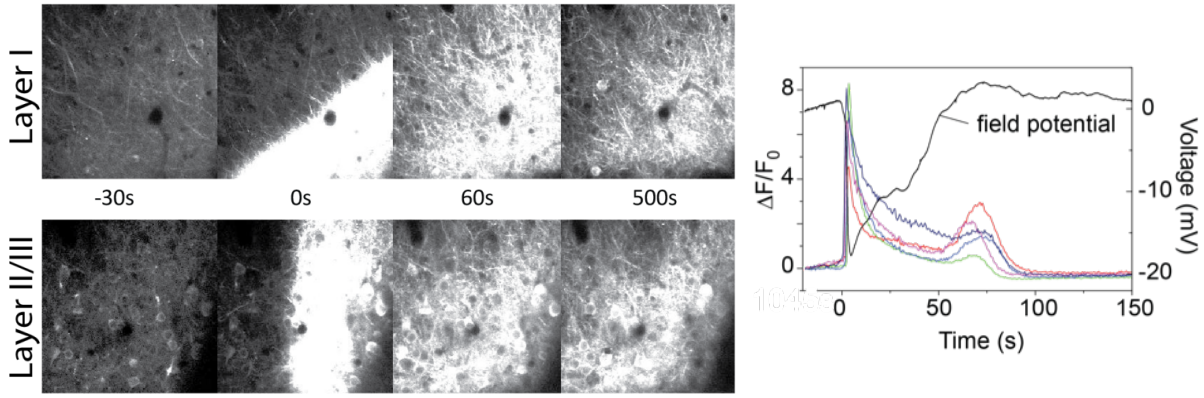

Figure 11: Layer specific calcium transients in neurons loaded with genetically encoded calcium indicator. An adeno-associated virus encoding GCaMP5 under the synapsin-1 promoter (neuronal specific) was injected in the cortex and 3 weeks later the mouse was prepared for imaging (craniotomy over somatosensory cortex). The same area was imaged at two different depths, corresponding to layer I and layer II/III. Sequences of images show the propagation of the CSD in these two different depths. Plot at right shows field potential (black) and calcium traces from five different neurons in layer 2/3. The calcium transient occurs simultaneous with the field potential depolarization.

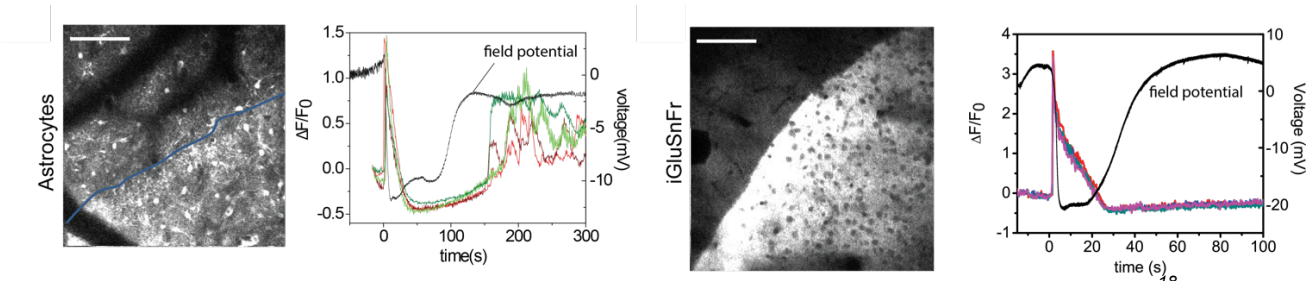

Figure 12: Genetically encoded astrocyte calcium indicator GfaABC1D.PI.cyto-GCaMP3 [18], and genetically encoded glutamate indicator iGluSnFr [19]. Both indicators show onset of activity coincident with field potential depolarization (downward black trace). However more detailed investigation revealed that astrocytic depolarization began before the onset of the CSD wave (see below). This surprising finding became a reportable outcome and is the basis for a manuscript in final preparation.

Neuronal two-photon imaging after TBI.

Two photon imaging after TBI has been technically challenging but ultimately successful. We initially used Oregon Green BAPTA multi-cell bolus loading, where an organic dye is injected acutely during the experiment 72 hours after CCI. Loading (5 animals) was much worse than in non-TBI animals, with very poor signal. This prompted the use of virus-delivered genetically-encoded calcium indicators. The indicator is injected 2 weeks before CCI in a burrhole 2-3 mm anteromedial to the CCI craniotomy, CCI is delivered, and animals are imaged 72 hours after CCI in a craniotomy between the burrhole and the CCI craniotomy. The combination of GECI and this craniotomy protocol has ultimately proved successful. However we must emphasize that obtaining this preparation was a major technical hurdle, and both failed dye loading and inability to achieve a viable craniotomy (due to blood and adhesions preventing removal of the skull without cortical damage) is a major issue.

Investigation of migraine mutant mice in parallel with wild type mice after TBI. Patients with migraine are more likely to develop post-traumatic headache after TBI[20]. Though this award did not proposed the use of migraine mice (no CDMRP funds are used for these mice), we are separately funded for this effort. We have thus conducted experiments on mutant and wild type mice together, as we believe this will provide deeper insight into the mechanisms of PTH in our service personnel, many of whom have migraine.

We use casein kinase 1 delta (CK1d) mutant mice[9] to compare with our wild type animals. A mutation in CK1d was identified in two families having sleep phase syndrome and typical migraine with aura. Mice genetically engineered to express this mutation showed a reduced threshold for CSD and an increased sensitivity to nitroglycerine induced mechanical and thermal hyperalgesia, both considered migraine relevant phenotypes[9]. Our hypothesis was that CK1d mice would have an amplified response to TBI compared to their wild type littermates.

Increased neuronal calcium load after TBI in CK1d mutant mice. We recorded calcium transients during CSD in WT and CK1d animals (5 in each group) 72 hours after sham or CCI (Figure 13). There were significant differences in all measures. The left figure panel shows calcium fluorescence maxima associated with CSD – these were significantly decreased after CCI in both groups – however in both sham and CCI animals, fluorescence maxima were significantly larger in CK1d animals. While fluorescence maxima were decreased after TBI, the duration of CSD associated calcium transients was significantly longer. The result is that the total calcium load (right panel; area under the curve of the calcium transient) was significantly greater after CCI than sham in CK1d animals ($p<0.05$, ANOVA with post-hoc Tukey Test), and significantly more variable ($p<0.05$, Levene's test) in WT animals. We interpret these findings as evidence of increased neuronal excitability after TBI, which is enhanced in animals carrying a migraine mutation. These results may help explain both the tendency toward headache and seizures after TBI, as well as the greater predisposition to PTH in patients with migraine.

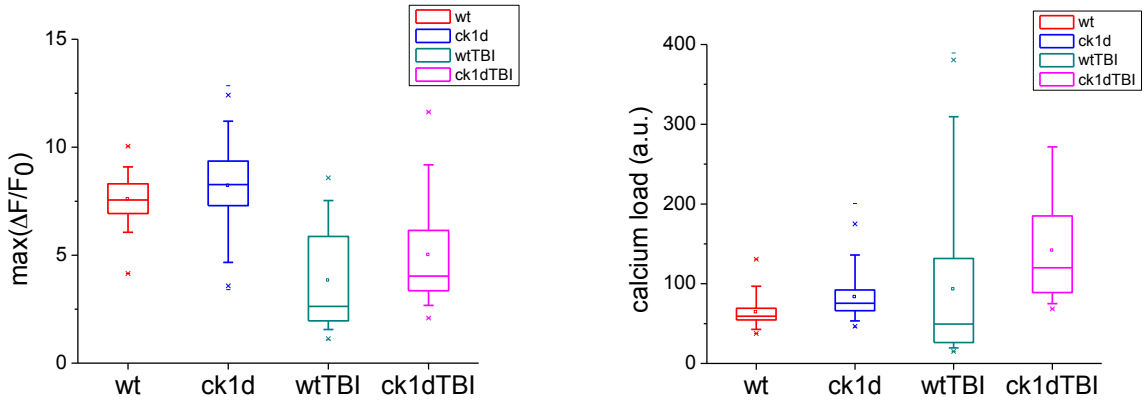

Figure 13: Calcium changes in WT and CK1d animals after CCI. WT and CK1d animals showed reduction in maximum calcium fluorescence observed in neurons following CCI, relative to sham animals. However, CK1d CCI animals showed larger maximum level of fluorescence, compared to WT CCI animals. Additionally, increased calcium load was observed in CK1d CCI compared to WT CCI animals.

In vivo *whole cell recording to determine the mechanisms of increased cortical excitability after TBI.*

To study functional changes in cortical neurons after traumatic brain injury, we have used *in vivo* whole cell electrophysiological recordings[21,22]. These recordings are able to dissect synaptic activity at the individual neuron level and thus amplify the resolving power of our two-photon recordings.

In vivo *whole cell recordings.* Mice were anesthetized using urethane (0.75 g/kg; i.p.) supplemented with isoflurane (~0.5 %). Body temperature was monitored and maintained at 37 - 38°C using a heating pad. Omega-shaped head bar was mounted on the skull, using glue and dental cement. Metal bar was screwed onto the holding rod, which was attached to the stage. A craniotomy 2 mm in diameter (as shown in Figure 14) close to the injury window was made (for sham treatment an injury window was made but no CCI was performed). The craniotomy was filled with 1.5-2% agarose (mixed in saline) in order to keep the cortical surface moist and dampen the movement associated with breathing. Neuronal recordings from approx. 1-1.5 mm from edge of lesion window were made. We used *in vivo* whole-cell techniques to record the membrane potential from layer 2/3 neurons in the mouse somatosensory cortex and analyzed spontaneous postsynaptic potentials (sPSPs) in the current-clamp mode at resting membrane potential (i.e., -65 to -70 mV).

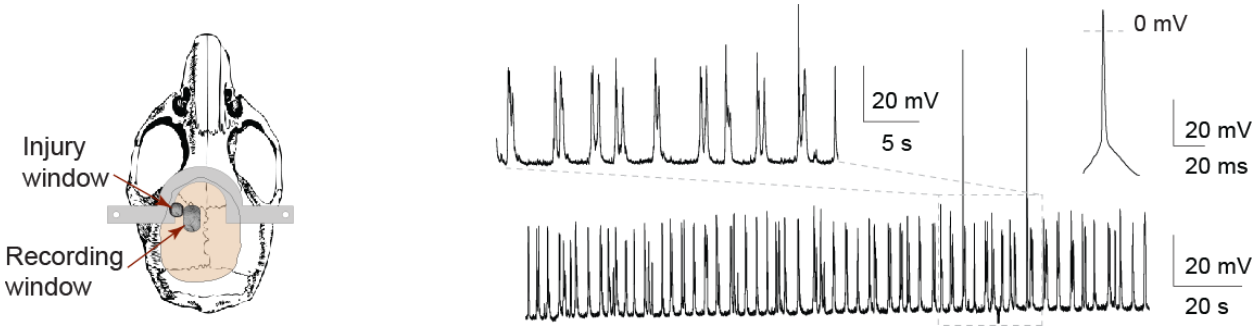

Figure 14: Schematic shows cranial window preparation for injury induction and recording site. Right: shows intracellular recordings of spontaneous upstates and downstates in urethane-anesthetized mice.

Intracellular recordings were performed using thick-wall glass pipettes pulled from borosilicate glass capillaries (OD 1.65 mm, ID 1.2 mm, Garner Glass, Claremont, CA) with a P-87 Flaming-Brown puller (Sutter Instruments, Novato, CA). Patch electrode of 4-6 MΩ was used (tip size of 3-4 μm). A patch pipette was filled with intracellular solution containing (in mM; pH = 7.2): 120 K-gluconate, 1 NaCl, 5 EGTA, 10 HEPES, 1 MgCl2, 1 CaCl2, 2 ATP. Signals were amplified using multiclamp 700B amplifier (Axon Instruments, Foster city, CA), sampled at 10 kHz, and low-passed filtered at 2 kHz. Data were acquired and stored on a PC using a Digidata-1320A digitizer (Clampex, Molecular Device, Union City, CA), and pClamp 8.2/10 software (Clampex, Molecular Device, Union City, CA).

Intrinsic membrane properties of neurons from WT and CK1d mice after sham and CCI

To examine whether the injury was associated with a change in the intrinsic membrane excitability, we analyzed resting membrane potential (RMP), input resistance, F-I slope, and rheobase (Figure 15). RMP was not changed significantly between WT and CK1d animals after sham or CCI treatments ($p > 0.05$, one-way ANOVA with Bonferroni's multiple comparison test; Figure 15A1). Input resistance was increased in transgenic naive, relative to WT naive animals (One-way ANOVA with Bonferroni's multiple comparisons, $p < 0.005$; Figure 15A2). However, no significant changes were observed after CCI or sham in either WT and CK1d animals.

No changes in rheobase were observed between WT and CK1d animals at baseline (naïve) and sham treatments. Rheobase of WT CCI neurons was not different than WT Sham animals however, CK1d CCI neurons showed increased rheobase relative to CK1d Sham neurons (One-way ANOVA with Bonferroni's multiple comparisons, $p < 0.005$; Figure 15A3). The slope of the frequency-current curve (measuring the frequency of action potentials in response to a series of intracellular depolarizing current pulses) was significantly decreased in CK1d CCI neurons, relative to CK1d Sham (One-way ANOVA with Bonferroni's multiple comparisons, $p < 0.005$; Figure 15A4).

Overall, CK1d neurons showed increased excitability (increased input resistance) at baseline. CK1d neurons showed reduced intrinsic excitability (increased rheobase, reduced F-I slope) after CCI, relative to sham CK1d neurons. However overall the changes in intrinsic excitability after TBI were relatively minor. We then considered measures of synaptic excitability, at baseline and after TBI.

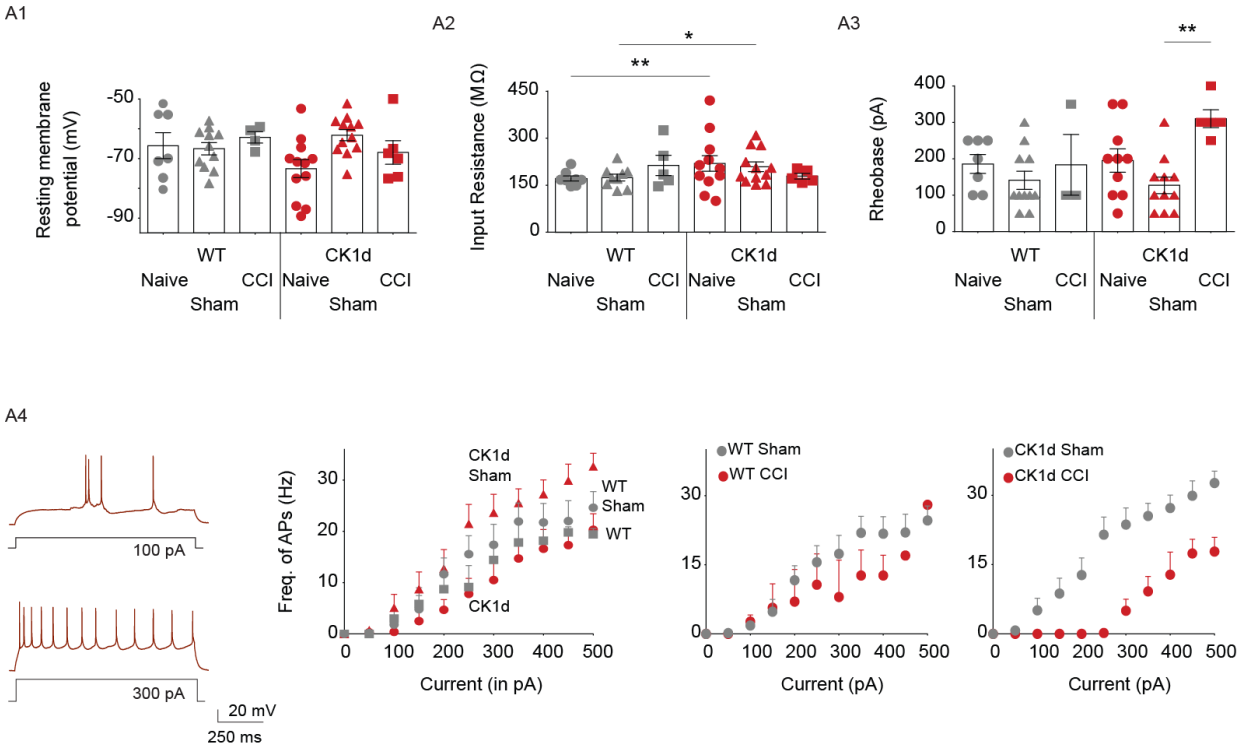

Figure 15: A1: No change in resting membrane potentials was observed after sham or CCI treatments in WT and CK1d animals. A2: The input resistance was increased in transgenic naive, relative to WT naive

animals. A3: Neurons from CK1d CCI animals showed increased rheobase, relative to CK1d Sham group. A4: Whole-cell recordings from pyramidal neurons showing action potential firing at two different current injections. The slope of the input-output curve (Frequency-current curve, F-I) for neurons from CK1d CCI animals showed a significant decrease in the F-I slope relative to CK1d Sham (One-way ANOVA with Bonferroni's multiple comparisons, $p < 0.005$).

Decreased frequency but increased amplitude, duration, and area of post-synaptic potentials in CK1d, relative to WT at baseline

First we assessed changes in cortical activity that included synaptic and network events between WT and CK1d neurons (Figure 16). We observed lower frequency of PSPs of neurons from CK1d animals, relative to neurons from WT animals ($p = 5.03e\text{-}07$; 2-sample KS test). However, amplitude ($p = 3.49e\text{-}05$), duration ($p = 1.95e\text{-}015$), and area ($1.26e\text{-}014$) of events shifted to the right, indicating increased amplitude, duration and area of those events in neurons from transgenic animals, relative to WT animals. Here again the findings are consistent with an increase in baseline excitability in CK1d animals compared to WT animals.

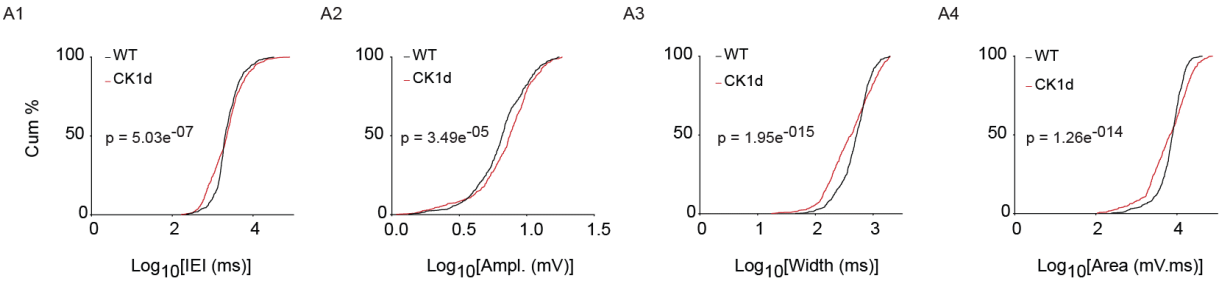

Figure 16: A1: Cumulative plot of intervals shifted to the right, showing lower frequency of PSPs of neurons from CK1d animals, relative to neurons from WT animals. A2: Amplitude of events shifted to the right, indicating increased amplitude events in neurons from transgenic animals. A3, A4: Distribution of duration and area of PSPs showed 75% of data in longer duration and larger area range in neurons from transgenic animals.

Increased frequency but reduced amplitude, duration, and area of post-synaptic potentials in CK1d vs WT animals 48 hours after sham CCI

Contrasting to CK1d versus WT neurons, comparing CK1d Sham to WT Sham neurons showed increased frequency ($p = 3.67e\text{-}04$, 2-sample KS test; Figure 17A1) but reduced amplitude ($p = 8.89e\text{-}17$), duration ($p = 1.66e\text{-}11$) and area ($p = 1.44e\text{-}12$) of PSPs. We interpret these results as another indication (see Subtask 1 above) that conventionally accepted sham treatments are not pure sham, and induce mild injury, likely through the craniotomy procedure.

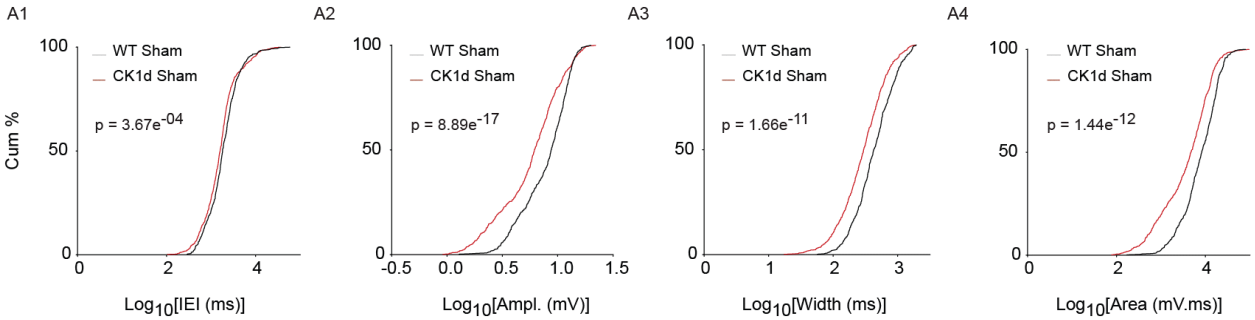

Figure 17: A1: Cumulative plot showing log transformation of interval shifted to the left, showing higher frequency of PSPs of neurons from CK1d sham animals, relative to neurons from WT sham animals. A2, A3, A4: Plots showing log transformation of amplitude, duration and area of events shifted to the left, indicating decreased amplitude, width and area of PSPs of neurons from transgenic sham animals.

Increased frequency but reduced amplitude, duration, and area of post-synaptic potentials in WT animals 48 hrs after CCI

To assess the potential involvement of synaptic changes following brain trauma, we analyzed the properties of spontaneous synaptic neurotransmission in the layer 2/3 cortical neurons. The plot of log intervals of the sPSPs for WT CCI group was significantly shifted to the left, suggesting decreased interevent interval and thus increased frequency (p = 6.84e-05, 2-sample KS test; Figure 18A1). The plot for log amplitude of the sPSPs in the WT CCI group was significantly shifted to the left, consistent with a reduced number of large-amplitude events (p = 7.17e-05; Figure 18 A2). Reduction in duration (p = 3.35e-22) and area (p = 2.15e-20) were observed in WT CCI neurons, relative to WT Sham animals (Figure 18 A3&A4). Study has shown 32% reduction in dendritic spines at 24 hours after CCI injury in layer 2/3 ipsilateral cortex (Winston et al., 2013) suggesting reduced density of glutamatergic post-synaptic receptors underlying reduced amplitude of PSPs. Increased glutamate levels in extracellular space have been observed in rat cortex within hours after CCI (Nilsson et al. 1994; Folkersma et al. 2011) and 24 hours after injury in humans (Chamoun et al. 2010), which may underlie increased frequency of PSPs.

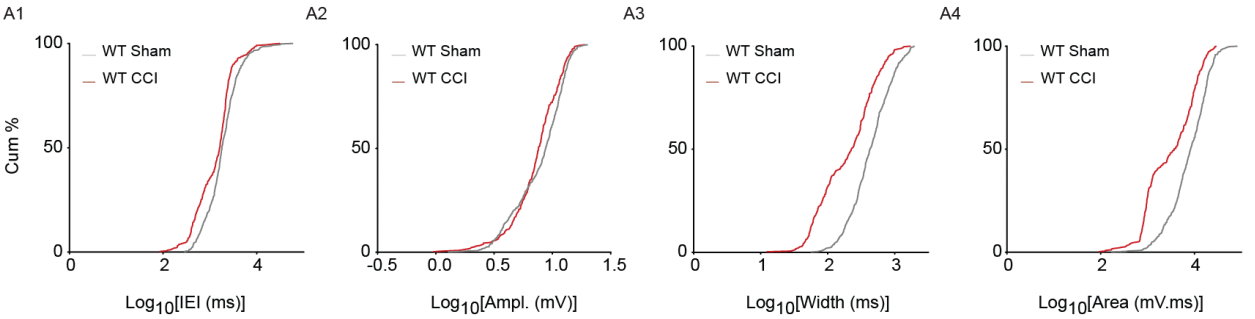

Figure 18: A1: Neurons from WT CCI showed higher frequency, compared to WT sham animals. A2: Compared to sham animals, CCI animals showed smaller amplitude events. A3: Reduction in duration of PSPs after CCI, relative to sham animals were observed. A4: Neurons from CCI animals showed significant reduction in the area, relative to sham.

Reduced frequency but increased duration and area of post-synaptic potentials in CK1d animals 48 hrs post-CCI

In striking contrast to WT animals CK1d CCI animals showed a significant *decrease* in the frequency (p = 1.39e-23; 2-sample KS test) but an increase in duration (p = 9.57e-04) and area (p = 3.64e-05) of sPSPs relative to WT CCI. These findings suggest a potentiation of post-synaptic responses leading to increased excitability after TBI (Figure 19).

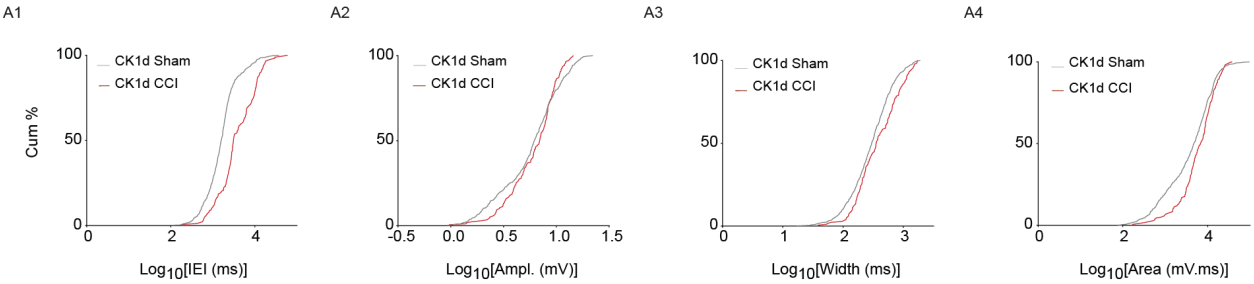

Figure 19: A1: Neurons from CCI animals showed reduced frequency of events, compared to neurons from CK1d sham animals. A2: No significant changes were observed in amplitude data between CK1d sham and CK1d CCI groups. A3, A4: An increase in PSPs duration and area after CCI, relative to CK1d sham animals was observed.

Decreased frequency and amplitude but increased duration and area of post-synaptic potentials in CK1d CCI, relative to WT CCI

A direct comparison CK1d CCI animals to WT animals after CCI showed a significant *increase* in the duration (p = 2.29e-11; 2-sample KS test) and area (p = 1.65e-10) of sPSPs relative to WT CCI (Figure 20). However, the frequency of PSPs was reduced in CK1d CCI, relative to WT CCI (p = 1.41e-24).

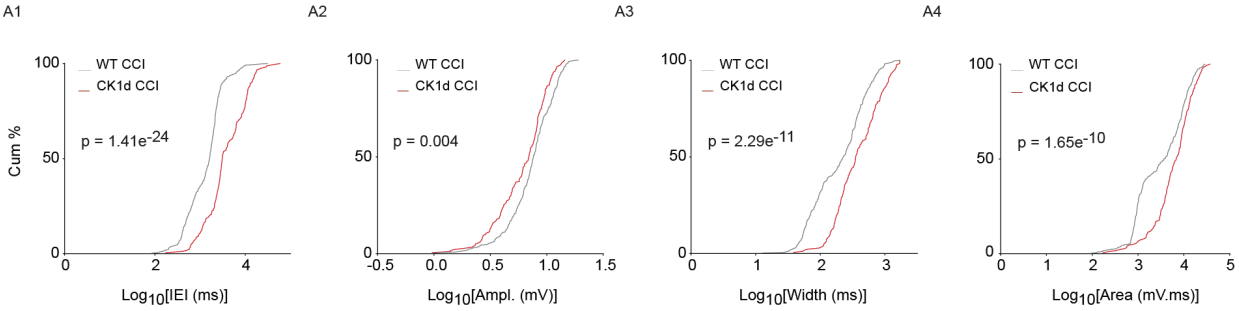

Figure 20: A1: Frequency was reduced in CK1d CCI group, compared to WT CCI group. A2: Amplitude was mildly reduced in CK1d CCI group. A3,A4: Cumulative plots of duration and area were shifted to the right, indicating longer duration and larger area of events in neurons from CK1d CCI, compared to WT CCI animals.

Summary of in vivo *whole cell data after TBI*

Our CCI data shows injury-induced increases in the frequency and decreases in the amplitude of sPSPs in layer 2/3 somatosensory neurons, 48 hrs post-injury, in WT animals. In contrast, larger amplitude and longer duration events were observed in CK1d mutants after CCI. These observations converge with our two-photon imaging data to suggest that traumatic brain injury

leads to cortical hyperexcitability in both CK1d and WT (to some extent) animals at 48 hrs after injury, but that migraine genotype is additive to the excitability phenotype, congruent with the increased susceptibility to PTH in migraineurs. These results may help explain why PTH is more common in migraineurs.

Subtask 4. Perform two-photon experiments 72 hours after lipopolysaccharide injection, acutely after hypotonic ACSF perfusion.

To ascertain the effect of a *low dose LPS injection* on cortical excitability, a group of 22 male animals was used to determine the effect of LPS exposure to CSD threshold. 6 WT and 6 KO animals were initially used to determine a baseline susceptibly of cortex to 1M KCl induced spreading depression. A subsequent group of 5 WT and 5 KO animals was injected with 0.5 mg/kg LPS i.p. The CSD susceptibility was measured 72 hours later. The CSD number following the first KCl induced event was recorded for 1 hour. The results are shown in Figure 21 (* = WT vs WT(LPS) P <0.05; # = WT(LPS) vs. KO(LPS) P<0.05 One-way ANOVA with post-hoc Tukey test). LPS treatment reveals a GFAP cell expressing-STAT3 dependent reduction in CSD number in KO animals, an observation not seen in the untreated group. These data show that *the immunological activation associated with TBI has effects on cortical excitability*. It appears that LPS-induced immunological activation reduces cortical excitability, in a manner that is dependent on astrocytic STAT3 signaling pathway function.

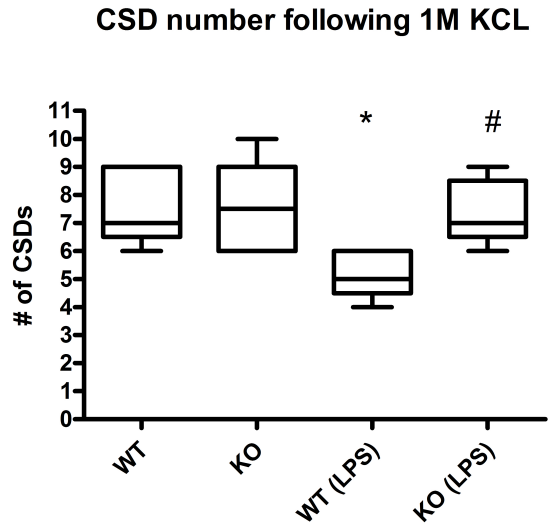

Figure 21:

To ascertain the effect on cortical excitability of *hypotonic ACSF perfusion*, 10 animals were implanted acutely with microdialysis probes (PlasticsOne, 13 kD membrane, 1mm length, 1mm depth into cortex) through a 2 mm craniotomy centered between bregma, lambda, sagittal suture, and temporal ridge. ACSF (in mM: 125 NaCl, 3 KCl, 1.25 NaH2PO4, 2 CaCl2, 1 MgCl2, 25 NaHCO3, 11 glucose, pH 7.4) was perfused at 0.1 ml/hr, either at full strength, half dilution with distilled water, 2/3 dilution with distilled water, or 100% distilled water perfusion. Reflectance

signal was collected from regions of interest between 100 - 200 μm of microdialysis probe, or > 1mm distant from probe. Next, the same regions of interest were recorded during CSD. There was no significant difference in amplitude of either spontaneous or CSD-associated signal at any region of interest at any concentration of ACSF. Moreover, placement of microdialysis probes made analysis of signal closer to probe problematic. Finally, attempts at performing two-photon experiments with the microdialysis probe were unsuccessful because it was impossible to approximate the microscope objective to the tissue with the probe in place. We concluded that, due to the low yield of reflectance imaging and the impossibility of carrying out two-photon experiments even if reflectance imaging had been promising, that further microdialysis experiments should be deferred.

Subtask 5. Perform histological analysis on animals 24, 48, 72 hours, and 7 days after CCI TBI.

Figure 22 shows the typical lesion pattern following our CCI protocol as well as Nissl stain of the CCI-lesioned region at different magnifications.

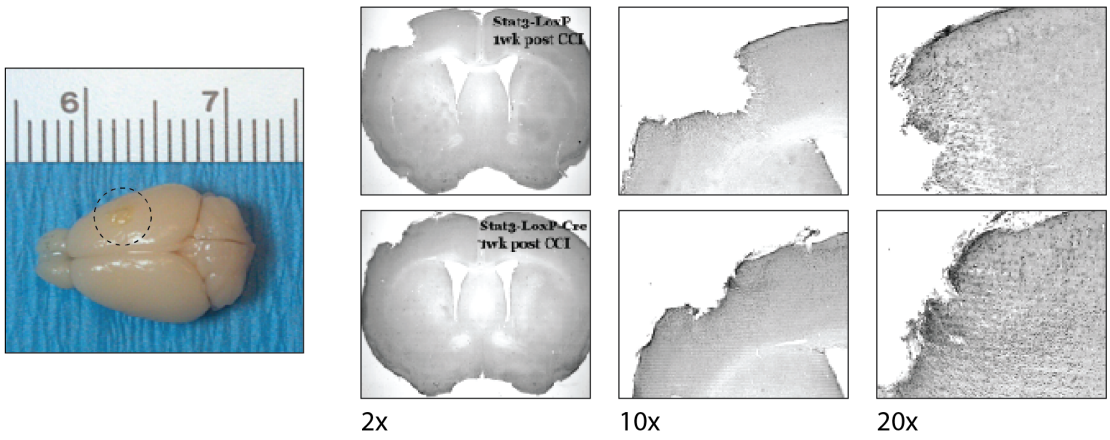

Figure 22: Typical brain after PBS and PFA perfusion, the CCI injury (circled) is approximately 2 mm in diameter. Light microscopy images of Nissl stain displaying lesion area 1 week following impact in WT (Stat3-LoxP) and KO (Stat3-LoxP-Cre).

Figure 23 shows neuronal (NeuN), microglial (Iba1), and astrocytic (GFAP) in tissue from the same anatomic location ipsilateral and contralateral to CCI. Neuronal numbers are not appreciably changed past the location of the glial scar. However there is a significant increase in astrocyte as well as microglial cell body and process size in the peri-contusion region but not the contralateral hemisphere, consistent with both astrocytic and microglial activation reported after TBI.

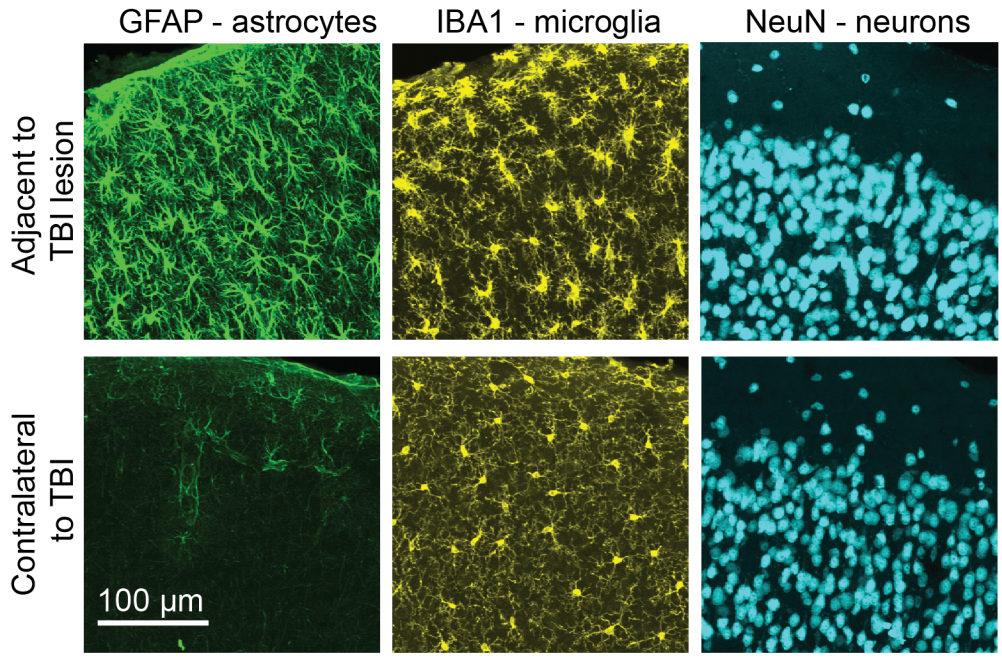

Figure 23: **Tissue effects of TBI.** A. Cortical sections of wild-type animals, 48 h after CCI TBI. Top images show cortex ipsilateral to the site of TBI, immediately adjacent to the lesion. Bottom images show contralateral cortex. There is an ipsilateral increase in GFAP staining and change in astrocyte morphology compared to contralateral cortex, suggestive of astrogliosis near the site of injury. Similarly, ipsilateral microglia (labeled with IBA1) appear to have a different morphology compared to those in the contralateral cortex. There is a mild increase in NeuN staining (labels neuronal nuclei) intensity ipsilaterally, but no clear change in morphology or number. Images shown are maximum intensity projections of approximately 20 optical sections through a single cortical slice.

Subtask 6. Perform plasma protein extravasation and brain water content experiments after TBI.

We used two-photon microscopy measurements to examine both plasma protein extravasation and brain water content with greater precision than possible with Evans Blue or brain weight measurements. Because of the complexity of post-CCI two-photon imaging, we used CSD as a TBI-relevant stimulus.

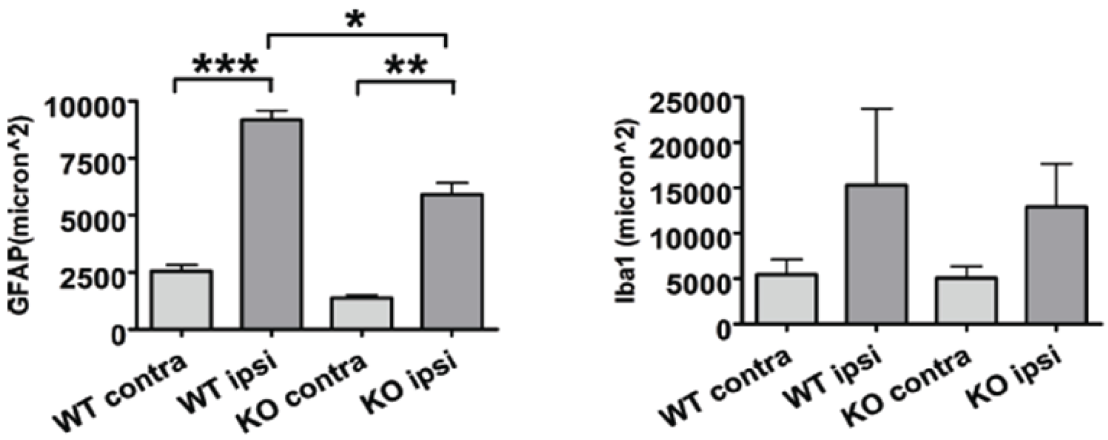

Figure 24: Quantification of GFAP and Iba1 expression after TBI in WT and STAT3 knockout mice. There is a significant increase in GFAP expression ipsilateral to CCI in both WT and KO animals, however the increase is significantly smaller in KO animals, consistent with an impaired astrocytic response. Iba1 expression shows a trend toward increase in both WT and KO animals. N=6 animals per group.

Measurements of vascular diameter, integrity, and metabolism

By injecting FITC-dextran dyes into the blood a real time quantification of the perfusion is accomplished (Figure 25**a,c**). Detailed imaging of the vessel wall can be obtained with Alexafluor633, which labels elastin filaments (Figure 25**b**). Because fluorescein dextran is too large to escape the blood vessel without blood-brain barrier breakdown, it can be used as a measure of vascular integrity and thus plasma protein extravasation. Finally, the intrinsic fluorescence of the cortex can be monitored providing information about the NAD/NADH ratio and thus the tissue metabolism which is ultimately governed by perfusion (Figure 26).

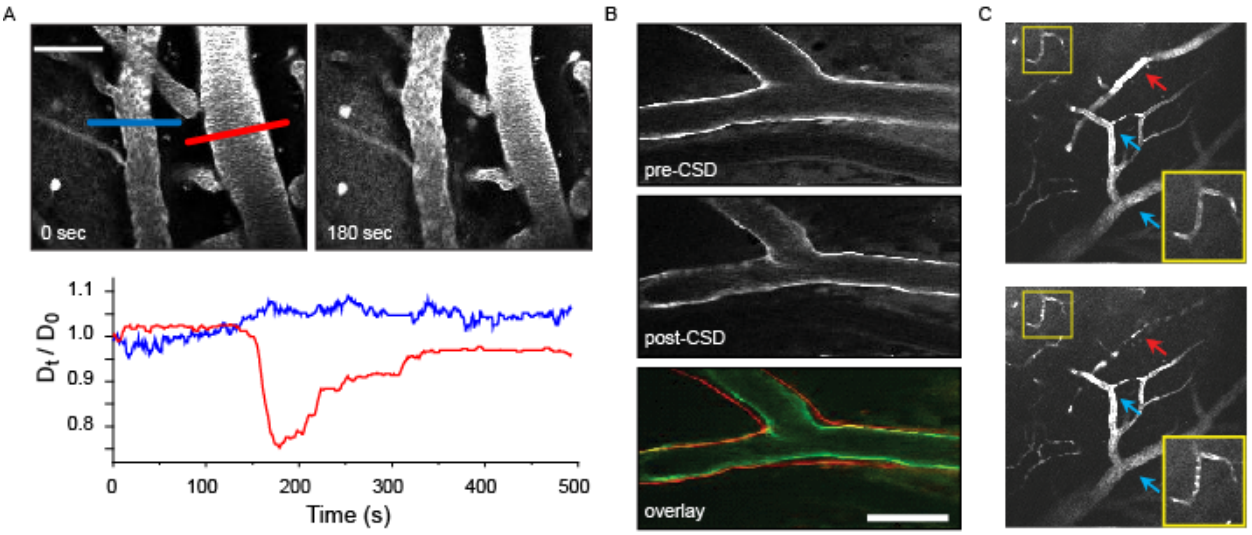

Figure 25: Massive vascular changes during and after CSD. A. Two photon images of a cortical artery and vein are shown before and during a CSD. Diameter changes were calculated across their cross-section (artery: red, vein: blue) and displayed as time traces in the plot below (scale bar, 50 µm). B. Arteries also undergo morphological changes (labeling of elastin fibers with AlexaFluor 633), becoming

more irregular (scale bar, 50 μm). C. Intracortical vascular dynamics during CSD. Images from 50 μm below the cortical surface show penetrating arteriole (red arrow), draining veins (blue arrows) and capillary (yellow inset). Plasma is labeled with 70 kD fluorescein dextran. At baseline, blood flow blurs individual red blood cells (RBCs). During CSD, arteriole (but not vein) constricts massively. Capillary blood flow stops, revealing individual RBCs as dark spots. Shortly after CSD passage, arteriole dilates beyond baseline, but capillary flow is still compromised. Scale: arrows are 50 μm long.

Despite very large changes in perfusion (red blood cell flux) and arterial diameter, we did not observe plasma protein extravasation (n=20). A caveat is that we measured primarily in layer 2/3 (15/20), and though we also measured in layer 1 (5/20), it is possible that with the different regulation of surface blood vessels[23] these might be a source of plasma protein extravasation that we did not observe.

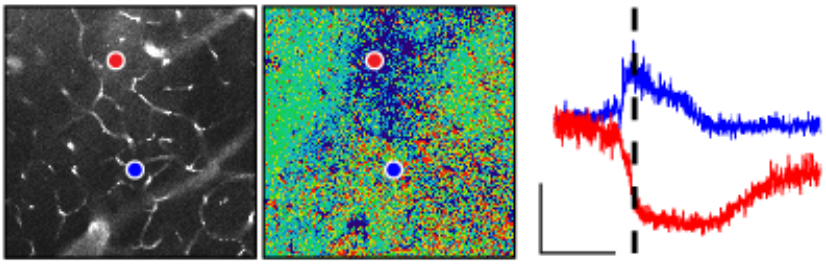

Figure 26: Fluorescein dextran labeled capillaries 250 μm below the cortical surface (left). NADH intrinsic fluorescence image from same location (center), during peak CSD-associated changes (dashed line on graph). NADH oxidation (red; darkening) and reduction (blue; brightening) can occur, depending on location, however most regions show reduction, consistent with the metabolic challenge of CSD. Calibration: 10% change from baseline; 45 seconds.

Massive but temporary tissue displacement, neuronal swelling, and dendritic beading with CSD.

Two-photon microscopy allowed us to quantify the changes that result in TBI-associated edema at cellular and subcellular resolution. We observed significant physical displacement (Figure 27) and neuronal swelling (Figure 28), as well as dendritic beading (Figure 29), but these lasted only for slightly longer than the duration of the CSD wave. We also observed much larger tissue displacement during CSD after TBI. A caveat here is that we could not directly capture peri-contusional edema – we made several attempts at this but because of bleeding and tissue adhesion in the boundaries of the CCI lesion we were unable to create viable cranial windows that would allow imaging.

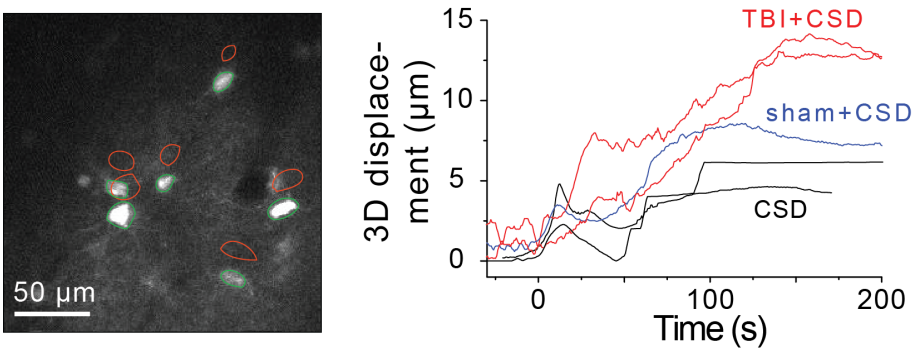

Figure 27: TBI increases mechanical displacement caused by CSD. Two-photon image (left) shows displacement of GFP labeled interneurons (layer 2/3) in the scanning plane for an animal 48 h after CCI TBI. CSD was induced by topical application of KCl. Red: pre-CSD position; Green: post-CSD position. Plot shows Euclidean distance calculated by a correlation-based algorithm for different animals. Red: mice with TBI 48 h before experimentally induced CSD; Blue: Sham TBI 48 h prior to CSD. Black: Mice with no TBI procedure.

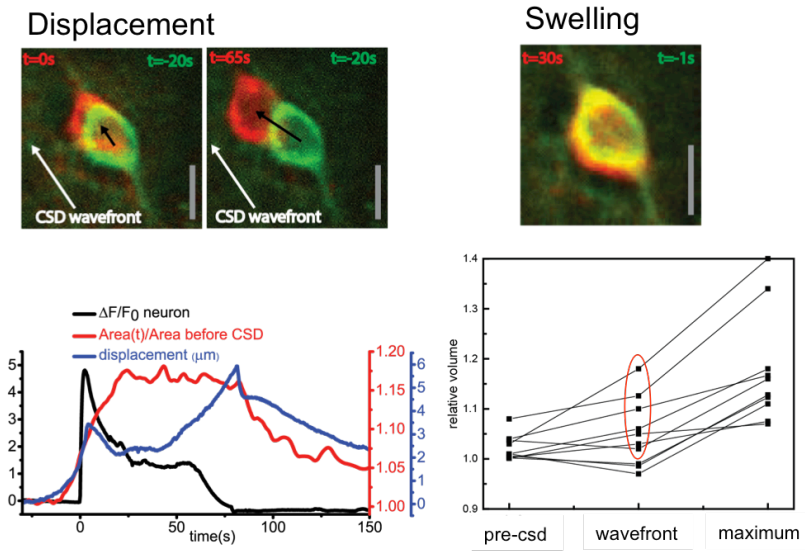

Figure 28: Top left: neuronal displacement occurs in two phases with passage of the CSD wave. Top right – same neuron swells by >50%. Bottom left: plot summarizes neuronal calcium (black), displacement (blue) and swelling (red). Bottom right: plot summarize neuronal volume changes. Note that neuronal volume changes begin before the onset of the calcium activity

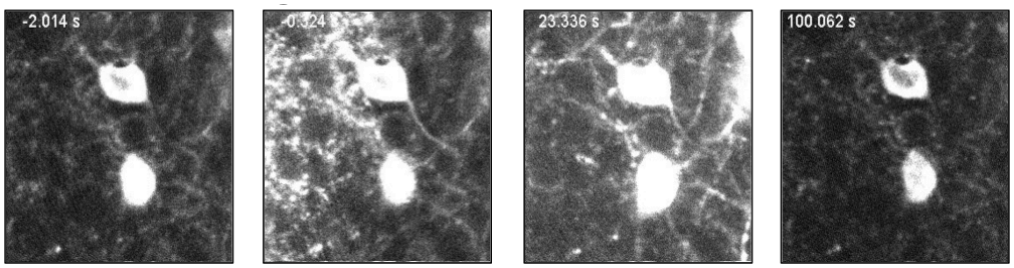

Figure 29: Prominent dendritic beading with passage of wave through tissue (visible as small round structures in dendritic tree, middle two images. Beading recovers shortly after passage of the wave.

Prodromal neuronal and astrocytic events anticipate and enable the CSD wavefront.

An unanticipated benefit of these experiments however is that they revealed events that occurred prior to the onset of the CSD wavefront. Note that in Figure 28 both displacement and neuronal volume changes (blue, red traces) start increasing approximately ten seconds *before* the onset of the CSD wavefront – represented by the black trace showing calcium activity. The events leading to CSD propagation are poorly understood, and these results challenged our current understanding. We followed up with combined *in vivo* whole cell and two-photon recordings to investigate further. We found that the change in neuronal volume coincided with a ramped increase in neuronal membrane potential, again before onset of wavefront-associated calcium activity and glutamate activity (Figure 30). These membrane potential changes thus cannot be caused by either calcium or glutamate. The only other candidate for this activity is extracellular potassium. Extracellular K+ can be measured, however at cellular resolution these recordings are confounded by the fact that the tip of a potassium electrode is much larger than the extracellular space, and thus temporal precision is lost. Indeed we found in K^+ electrode recordings (not shown) that extracellular [K+] rises varied in timing with the CSD wavefront.

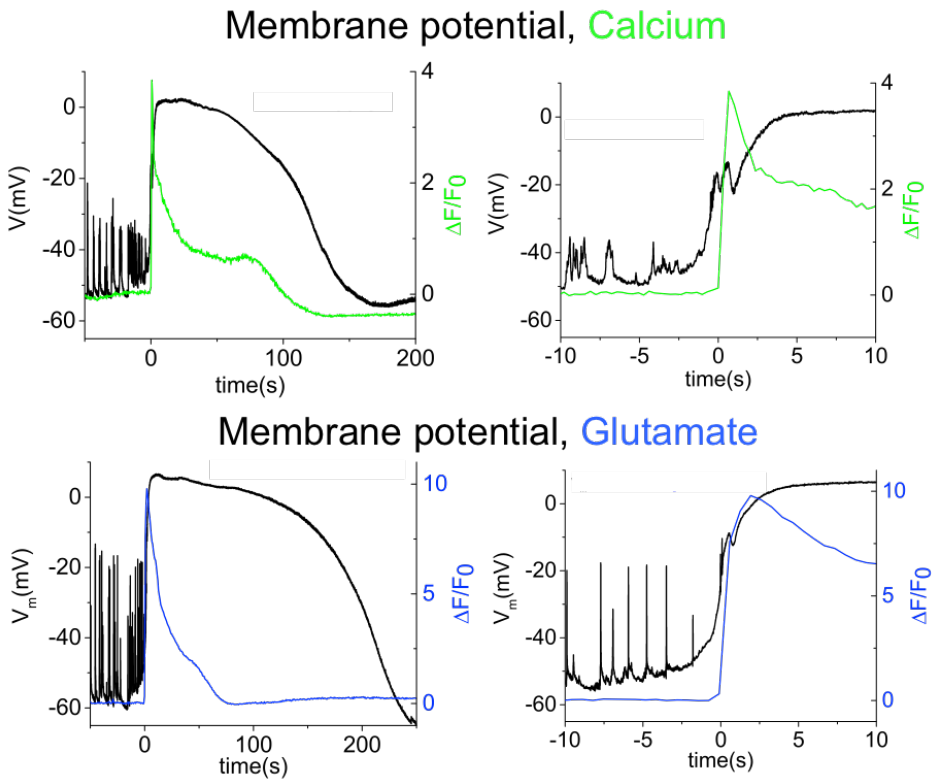

Figure 30: Combined in vivo whole cell recordings and neuronal calcium (green, above) and glutamate (blue, below) recordings show that neuronal membrane potential increases before the onset of the calcium or glutamate CSD wavefront. Compare with Figure 12, which show calcium and glutamate coinciding with the extracellular DC field potential shift, the gold standard delimiter of the CSD wavefront.

However, due to very high expression in astrocytes of K^+ channels that are open at negative resting voltages, the astrocyte passive conductance is essentially K^+ -selective and the astrocyte membrane potential behaves as a good K^+ electrode, rendering astrocytes useful cellular resolution [K^+] biosensors[24–26]. We combined *in vivo* whole cell recording and calcium imaging from *astrocytes* to determine whether there were pre-wavefront changes. Figure 31 shows averaged CSD associated calcium activity from 100 cells (left, inset at bottom left) showing rises in astrocyte calcium activity that begin >40 seconds before the wavefront. Combined neuronal calcium and immediately adjacent astrocyte whole cell recordings (representative recording at right) show a ramped depolarization of astrocyte membrane potential beginning >50 seconds before the neuronal calcium-determined CSD wavefront.

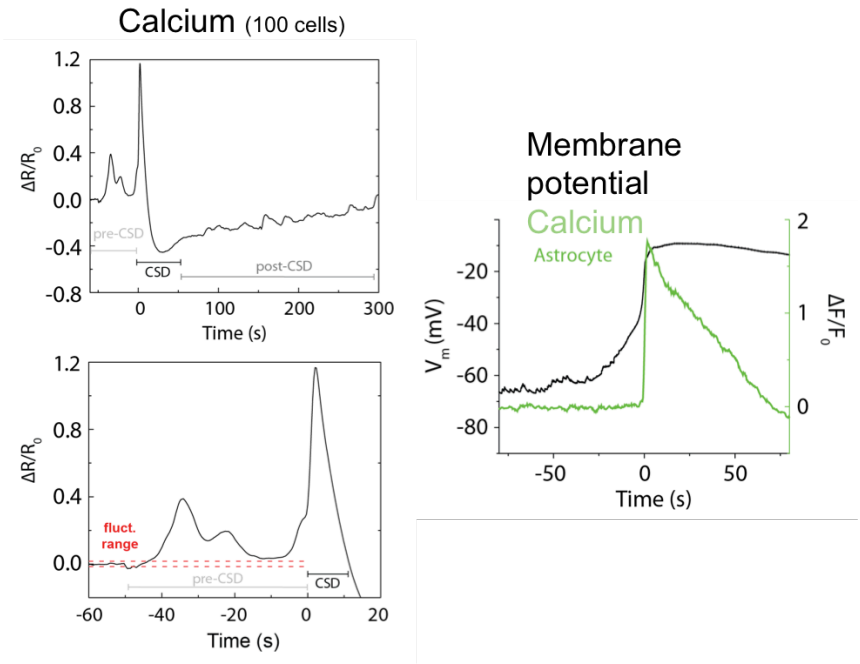

Figure 31 Astrocyte calcium and membrane potential changes tens of seconds before CSD wavefront. Top left: average calcium traces from 100 astroctes show significant activation above baseline fluctuation range (red in lower inset) that begin >40 seconds before the astrocyte CSD wavefront (compare with Figure 12, which shows coincidence of astrocyte wavefront and DC field potential shift). Right: astrocyte membrane potential rises >50 seconds before an immediately adjacent neuron's calcium wavefront.

We interpreted these findings to mean that extracellular K^+, sensed and likely buffered by astrocytes, causes changes in astroyctic networks tens of seconds before any neuronal activity or the CSD wavefront. As K^+ increases, astrocyte buffering fails, likely leading to the progressive neuronal membrane potential changes that precede the wavefront. These in turn lead to a burst of action potentials that heralds the steep rise in membrane potential, glutamate release, and calcium activity that represent the CSD wavefront.

These unanticipated findings, arising from our work on vascular integrity and neuronal volume at cellular resolution, are in final stages of preparation for a manuscript that will we hope will significantly increase the understanding of TBI-associated depolarizations.

Subtask 7. Analyze results, correlate with histological and other experimental data, prepare data for publication.

Analysis shown for each task in context.

Specific Aim 2:
Determine whether the chronic post-TBI state is marked by cortical excitability and behavior consistent with migraine and epilepsy

Major Task 2. Chronic experiments after CCI TBI (Brennan, Dudek, Months 1-48).

Subtask 1. Perform CCI, implant monitoring device, and monitor for chronic effects of TBI.

See Major Task 1 – experiments spanned both acute and chronic time course continuously.

Subtask 2. Perform voltage sensitive dye experiments 3 months after CCI.

We performed preliminary experiments to optimize VSDI acquisition in our new lab location. Though we had no difficulty performing the experiments in uninjured animals (Figure 32), we found that the RH1691 dye used to generate fluorescence on cortical depolarization adhered to injured tissue in a way that resulted in artifactual, static high fluorescence. This degraded our ability to detect neuronally induced signals. We discontinued any further VSDI experiments with the rationale that they were not feasible in brain injury preparations, at least in our hands.

However we realized that our *in vivo* whole cell recordings provide a far superior record of membrane excitability (albeit for a single cell at a time). We are now using *in vivo* whole cell recording at chronic time points after TBI to examine long-term effects of TBI on neuronal membrane excitability (CDMRP PR 130373). Thus, though VSDI has proven unviable, the main scientific question underlying this Subtask is being pursued.

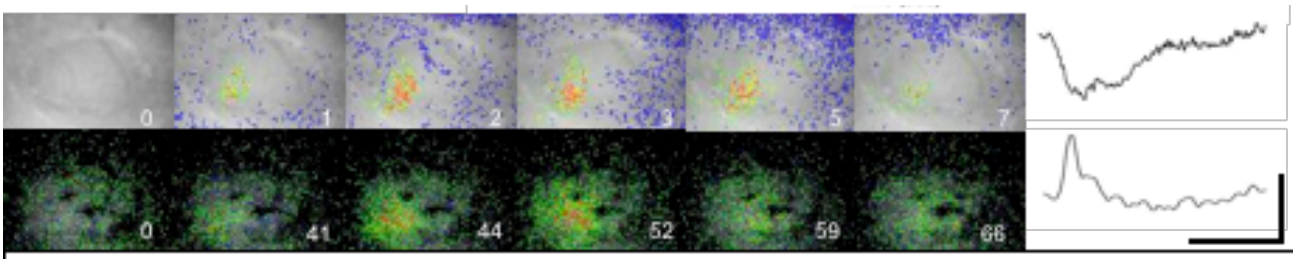

Figure 32: **Cortical mapping with OIS and voltage sensitive dye imaging (VSDI).** Hindpaw representation elicited with OIS (top) and VSDI (bottom) in same animal. OIS trace is average of 10 stimulus trains; VSDI trace is response to one stimulus. Area of map is similar but time scale is very different. OIS time labels are seconds; VSDI labels are milliseconds. Traces show timecourse of signal. Scale bar: Horizontal: 4 sec. for OIS, 100 msec. for VSDI. Vertical: 0.1% for OIS; 0.4% for VSDI

Subtask 3. Perform CCI, two-photon experiments 3 months after CCI.

Obtaining viable cortical windows 3 months after TBI has been very difficult due to the near universal generation of adhesions around the injury margins. Adhesions prevent the removal of the skull to create a cranial window in the area around the injury – removal of adhesions generates its own acute injury. We are currently using blast injury (CDMRP PR130373) which should avoid this issue. However given the universal occurrence of CSD with CCI TBI, we have also used CSD as a proxy for epilepsy- and post-traumatic headache relevant aspects of TBI. CSD may not simulate all aspects of TBI, but as an essential component of the process we know that the effects it engenders are likely to be at play in the post-TBI state.

Long-term plasticity induced by TBI-associated CSD

We have previously shown that CSD identical to what we have observed in TBI induces changes in evoked sensory response consistent with long-term potentiation and depression[27]. We suspected that the CSD induced with TBI would cause similar changes, and we were able to investigate this at the cellular level using *in vivo* whole cell recordings. We found that CSD caused a reduction in spontaneous synaptic activity and action potential firing that lasted over an hour. Both pre- and postsynaptic mechanisms contributed to this silencing: Reductions in frequency of postsynaptic potentials were due to a reduction in presynaptic transmitter release probability as well as reduced action potential activity. Decreases in postsynaptic potential amplitude were due to an inhibitory shift in the ratio of excitatory and inhibitory postsynaptic currents. This inhibitory shift in turn contributed to the reduced frequency of action potentials (Figure 33). Most of these changes lasted longer than the duration of our experiments, consistent with entrainment of long-term plasticity mechanisms after TBI-associated CSD (Figure 34). These results are under revision at Cerebral Cortex.

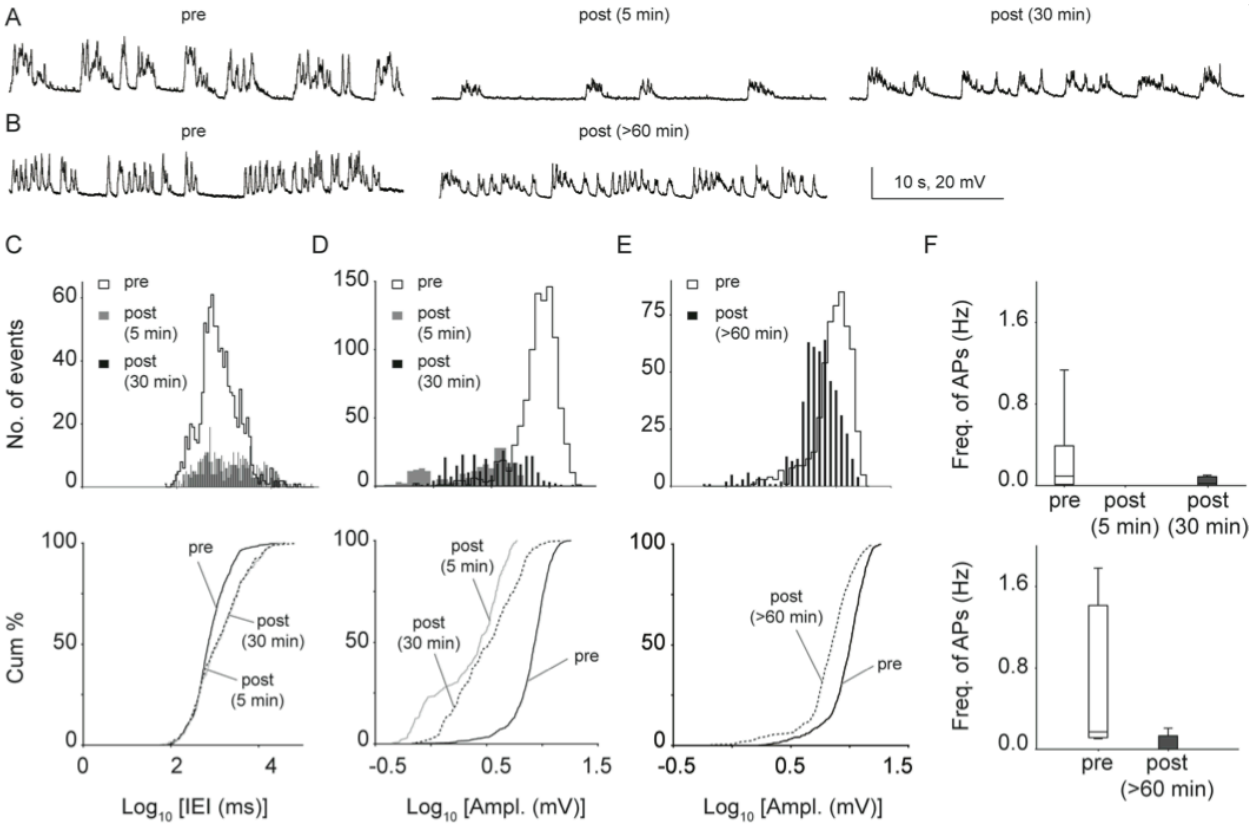

Figure 33: Significant reductions in spontaneous synaptic activity and action potential firing more than 1 hour after CSD in vivo. (A) Consecutive membrane voltage traces (30-s) from continuous recordings of spontaneous postsynaptic potentials (sPSPs) before, and 5, and 30 min after CSD from the same cell. There is a dramatic reduction in sPSP amplitude and frequency 5 min after CSD, which recovers but remains below baseline 30 min after the event. (B) Similar traces comparing a cell patched before CSD to a separate cell patched >60 min after CSD in the same animal. (C,D) sPSP amplitude and frequency were significantly reduced 5 and 30 min after CSD when recorded from the same cell. (Histograms above; cumulative plots below. Amplitude: 5 min: $p = 2.01*10^{-12}$; 30 min: $p = 2.77*10^{-8}$, 2-sample KS test; Frequency: 5 min: $p = 3.78*10^{-8}$; 30 min: $p = 4.59*10^{-10}$, 2-sample KS test; n = 6 cells, 6 mice). Similar changes were seen at 30 min comparing cells recorded before to separate cells recorded 30 min after CSD from the same animal showing that findings were not due to rundown of whole cell recordings. (E) Recordings comparing cells recorded before to separate cells recorded >60 min after CSD in the same animal: there was no significant difference in sPSP frequency at this time point ($p > 0.05$, 5 cells, 5 mice, 2-sample KS test; not shown); however amplitude of PSPs remained reduced for at least 90 min after CSD ($p = 3.86*10^{-40}$; 5 cells, 5 mice; 2-sample KS test). (F) Box-whisker plot showing no AP firing at 5 min post-CSD and significantly reduced AP firing 30 (upper panel) and >60 min post-CSD (lower panel).

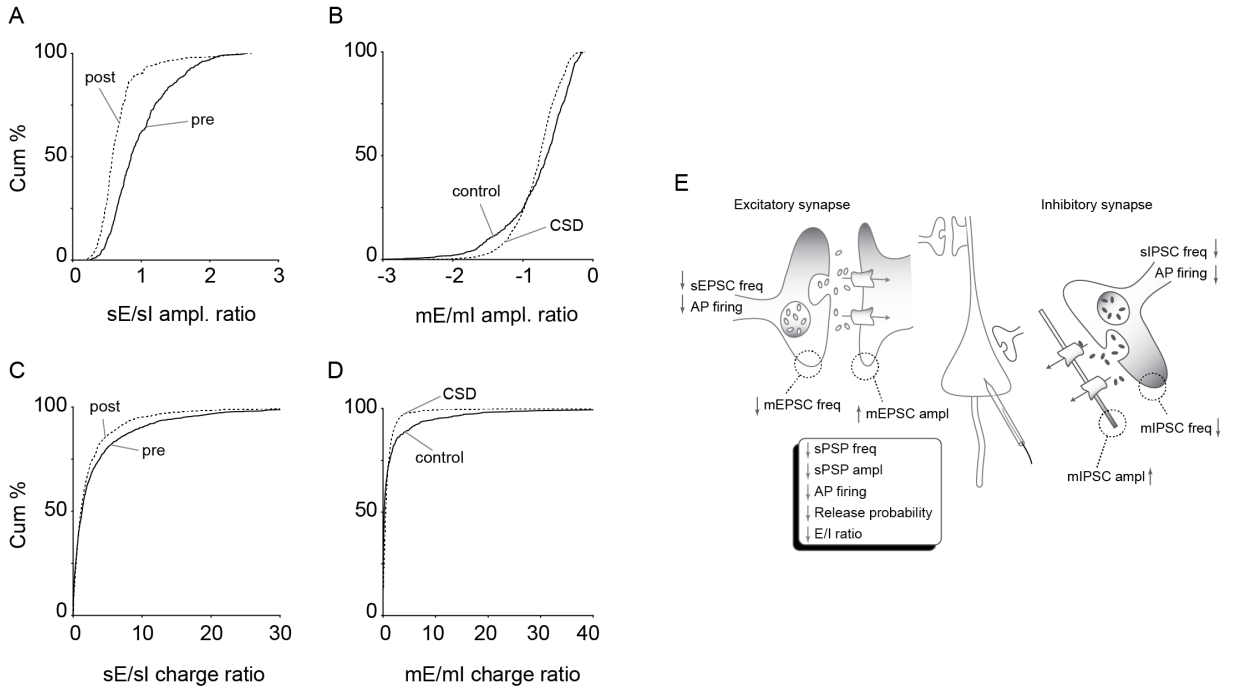

Figure 34: Inhibitory shift in excitation/inhibition ratio after CSD. Different measures of excitation/inhibition balance all show inhibitory shift 30 min after CSD. (A) Decrease in ratio of sEPSC to sIPSC amplitude ($p = 2.59*10^{-24}$, KS-test) in post-CSD group. (B) Decrease in ratio mEPSC to mIPSC amplitude ($p = 2.51*10^{-12}$, 2-sample KS test). (C) Decrease in ratio of sEPSC to sIPSC charge ($p = 0.004$, KS test). (D) Decrease in ratio of mEPSC to mIPSC charge ($p = 1.08*10^{-17}$; 2-sample KS test). (E) Schematic shows summary of intrinsic and synaptic changes 30 min after CSD. Box summarizes overall findings. Presynaptic decrease in AP firing and release probability combine with a postsynaptic inhibitory shift in excitation/inhibition ratio to generate the sustained depression in neuronal activity observed after CSD.

Long-term interneuronal plasticity induced by CSD.

We have also used two-photon microscoy with genetically encoded interneuronal indicators (Gad2-CCaMP3) to examine long term effects on this cell population, which is essential to generation of sensory maps as well as regulation of excitatory activity. We found that CSD elicited two days after an original CSD exposure involved repetitive interneuronal activity that was never seen in control animals –a clear demonstration that long-term changes in interneuronal function had been entrained (Figure 35). We are actively investigating the mechanism of these changes – from a teleological standpoint they make sense, as increases in interneuronal activity would be expected to dampen TBI/CSD associated excitability increases.

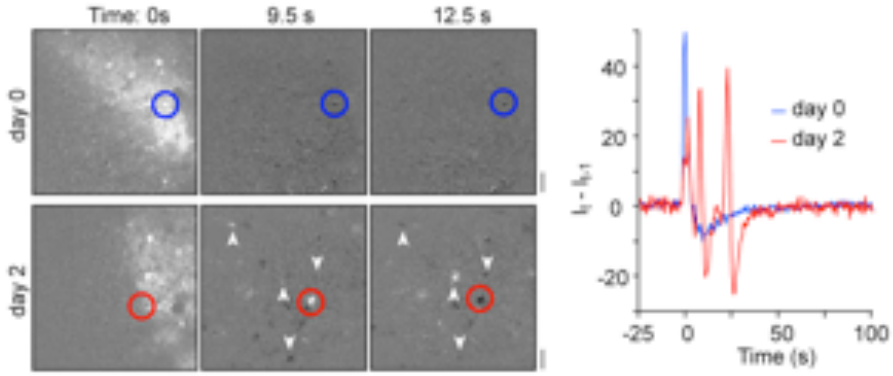

Figure 35: Evidence of interneuron plasticity on repetitive CSD. A Gad2-GCaMP3 animal was prepared with a chronic optical window for consecutive imaging over several days. Difference images (It-It-1) show CSD wavefront (time: 0s) and frames following CSD. Regions of interest over cell bodies (circled) are plotted showing repetitive high amplitude discharges that were present in the majority of cells (arrows) on day 2 but were not present in any cells after CSD on day 0 (confirmed in 2 Gad2-GCaMP3 acute experiments). These findings are direct evidence of CSD-induced neuronal plasticity on long time scales. Scale bars: 50 μm.

Subtask 4. Perform histological analysis on animals 3 months after CCI TBI.

Examining neuronal death with FluoroJade B staining

48 hours or 14 days after CCI or sham surgery, animal was anesthetized with isoflurane and then perfused transcardially with cold phosphate buffered saline (PBS) followed by a fixative containing 4% paraformaldehyde (PFA) in PBS. After the brain was removed, it was postfixed in PFA for 24 hours and then stored in PBS until it was sectioned. Coronal sections in 30 µm thickness were cut using a cryostat (Leica) and mounted on Superfrost/Plus slides. The sections were then processed for FJB analysis. Briefly, these sections were incubated in following solutions: 100% alcohol, 3 min; 70% alcohol, 1 min; distilled water, 1 min; 0.06% potassium permanganate, 15 min; dH2O, 1 min; 0.001% Fluoro-Jade B in 0.09% acetic acid, 30 min; dH20, 3 times, 1 min. Stained sections were dried at room temperature overnight, were immersed in xylenes and then cover slips were applied using DPX mounting media. FJB-stained slices were imaged using a Hamamatsu Nanozoomer 2.0 HT (Olympus) at 20X magnification.

We analyzed brain damage in mice at 48 hr and 14 days post-CCI. Histological examination of sections exhibited that CCI injury produced moderate level of focal lesion in the ipsilateral somatosensory cortex at 48 hr and 14 days after injury. Cortex lost its normal conformation at the concussion site, specifically a cavity was observed with irregular edges that did not extend to the subcortical structures mainly hippocampus (Figure 36). Examination of the whole brain (+1 mm anterior and 2 mm posterior to bregma) sections revealed that at 48 hr and 14 days after CCI the lesion size spanned from Anterior/Posterior +1.0 to -1.5 mm from bregma. This progression of lesion was not observed in the sham animals.

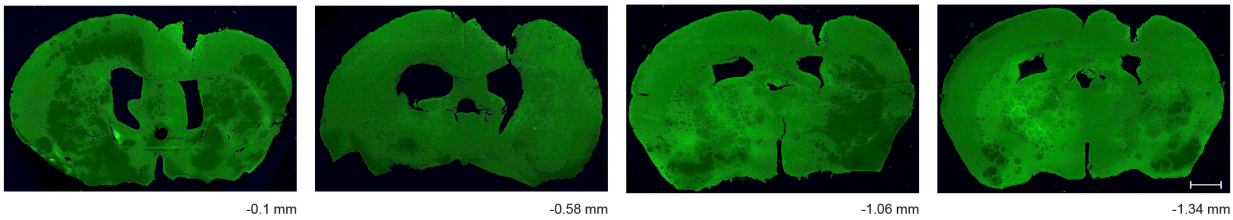

Figure 36: Typical example of cortical lesion in an injured mouse brain at 48 hrs post-injury. Injury was at peak at Bregma -0.58 mm. Scale bar = 1 mm.

The graph in Figure 37 shows that the area of cortical contusion lesion in the ipsilateral cortex as a percentage of the contralateral uninjured cortex was 11.23% in WT CCI group (n = 4 animals), whereas the area of lesion was 9.72% in the CK1dCCI group (n = 3 animals) at 48 hr post-injury. No animals from sham treated animals showed lesion in the ipsilateral cortical side relative to contralateral (CK1d Sham: n = 5 and WT Sham: 3). No significant changes in lesion area was detected between WT and CK1d CCI groups (unpaired t-test: $p > 0.05$).

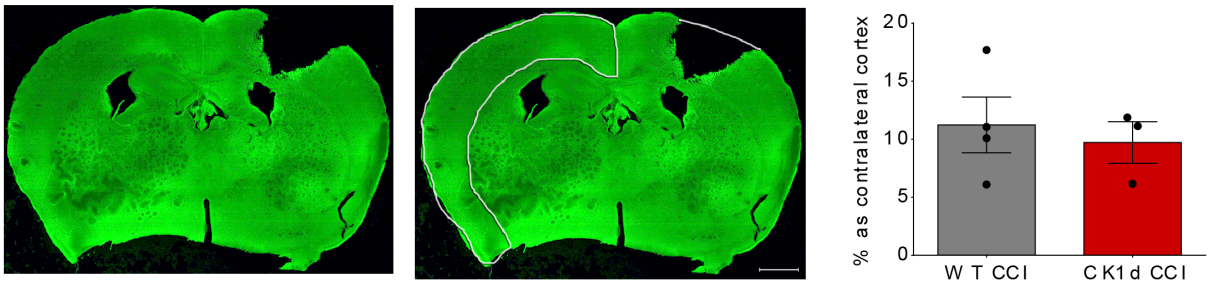

Figure 37: Top: Shows the method for analyzing the cortical contusion area in the ipsilateral hemisphere relative to the area of contralateral cortex. Cross-section of the brain showing injury of the controlled cortical impact at 48 hrs at the coordinate of -1.0 mm from bregma. Section shows a cortical cavity at the injury site. Middle: Area of the cortical contusion was measured by dividing area in the ipsilateral cortex (as shown in white outline) by area in the contralateral cortex (as shown in white outline). Scale bar = 1 mm. Bottom: Graph shows the percentage area of cortical contusion in the ipsilateral cortex relative to the area of the contralateral cortex. Data shows average of three sections that showed highest level of lesion. The brains were stained with FluroJade.

At 14 days after CCI, one animal out of 3 CK1d CCI group and one animal out of 2 WT CCI group showed no lesion. As expected, sham-treated animals also showed no obvious lesion in the ipsilateral area.

To examine neuronal damage, we used Fluoro-Jade B (a marker for neuronal degeneration) staining. Analysis of Fluoro-Jade staining indicated that there was significant cell degeneration at 48 hr after controlled cortical impact injury (Figure 38). Robust FJB-positive labeling, indicative of damaged neurons and degenerating processes, are observed in the ipsilateral cortex whereas the contralateral cortex was unlabeled. Staining was mostly apparent in the perilesional area (i.e., around the lesion site). However, at 14 days after injury, no cell necrosis was observed, suggesting a transient process of neuronal degeneration in cortex. All layers of ipsilateral cortex showed neuronal damage and no layer-specific pattern of degeneration was observed.

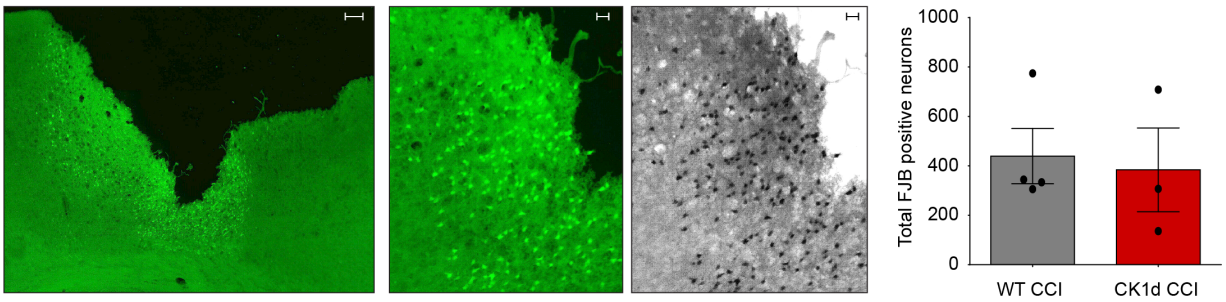

Figure 38: Top: Shows detailed cortical cavity surrounded by degenerating neurons labeled, using Flurojade staining. Scale bar = 250 µm. Middle: Fluoro-Jade B fluorescent neurons in the hippocampus following TBI. Sections are from animals that were sacrificed at 48 hrs after injury. Note the higher number of Fluoro-Jade positive neurons in perilesional area of injury in all layers of cortex. Analysis of FJB staining at 14 days after injury showed no sign of cell loss/necrosis in the somatosensory cortical region (data not shown). Calibration bar = 20 µm. Bottom: The total number of Fluoro-Jade B positive neurons in the ipsilateral cortex, mainly in the perilesional area of injury following CCI. At 2 days following injury, significant numbers of positive neurons were observed in the ipsilateral cortex. Data shows

average staining of positive neurons from three sections that showed highest level of lesion. No significant differences were observed between WT CCI and CK1d CCI groups (Unpaired t-test, $p > 0.05$).

Subtask 5. Perform plasma protein extravasation and brain water content experiments, analysis on animals 3 months after CCI TBI.

Please see Specific Aim 1, Subtask 6 above.

Subtask 6. Perform nociception behavior experiments (mechanical and thermal thresholds, rotarod) on animals 3 months after CCI TBI.

We have experience with both mechanical and thermal hyperalgesia testing; we realized that to have the clearest picture of headache relevant behavior (and potential confounds) after TBI, we needed to nest hyperalgesia testing in a more comprehensive behavioral phenotyping regimen. This regimen consists of open field testing to test for locomotor behavior, anxiety, and spontaneous behavior in general; then elevated plus maze testing to examine anxiety and also possible photophobic behavior; followed by testing of mechanical hyperalgesia after nitroglycerin, at 72 hour and 3 month time points. A particular reason to test more broadly is that stress (which is likely after TBI in both animals and humans) is associated with pain behavior and could confound results if not measured specifically. Our combined general behavior/stress/pain metrics allows us to correlate the measures and gain a more nuanced picture of the overall response. After the behavioral regimen all animals also undergo CSD testing to evaluate whether PTH-relevant cortical excitability is altered.

We first aimed to evaluate whether there is a difference in exploration/locomotion and stress responses in CK1d+ vs. their WT counterparts after CCI vs. sham treatment. We have evaluated the animals 48 and 72 hours after sham or CCI using the open field and elevated plus maze tests respectively.
CK1d+ after CCI showed an increase in both the distance travelled (Figure 39a) and maximal speed (Figure 39c) in the open field test compared to sham controls indicating a significant increase in mobility. Their WT counterparts however, showed a reversed phenotype indicated by a significant reduction in both distance travelled (Figure 39a) and maximal speed (Figure 39c) compared to their sham controls. This indicates a reduction in mobility for CK1d WT compared to a reversed phenotype for CK1d+ male mice following CCI. When evaluated 30 days after CCI, CK1d+ did not show any change in mobility compared to their sham controls in both distance travelled and maximal speed. Both CK1d+ and their WT counterparts did not show signs of increased anxiety compared to sham controls as shown by their similar time spent in the center of the open field arena.

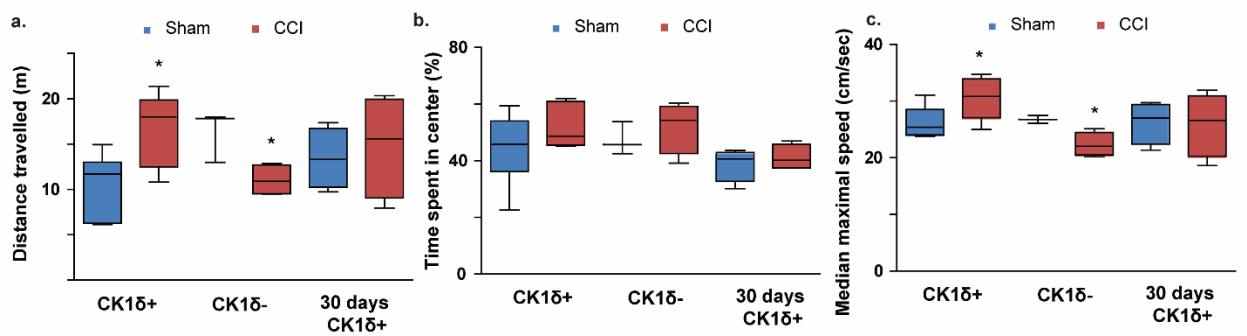

Figure 39: Box whisker plots representing activity in the open field test for CK1d+, CK1d- (WT counterparts) and CK1d+ 30 days, after CCI vs. sham treatment. In all graphs, boxes represent median (75th and 25th percentile), and whiskers represent max and min values per each group. **a.** Total distance travelled during 30 min test for each mouse. CK1d+ after CCI showed a significant increase in total distance travelled, while CK1d- showed a significant decrease compared to sham controls. The difference seen for CK1d+ was not seen when evaluated 30 days after CCI and sham. **b.** Percent time spent in the center of the arena. No significant difference was seen for either of the tested groups between CCI and sham controls. **c.** median maximal speed during mouse progression was seen to be significantly increased after CCI for CK1d+ but decreased for CK1d-. This increase was not seen for CK1d+ 30 days after CCI and sham. (*p<0.05, Student's t-test, n=7 per group for CK1d+; n= 3, 4 for CK1d- sham and CCI respectively; n=4 per group for 30 days CK1d+).

We also wanted to see if female CK1d+ showed similar increased mobility after CCI as seen for male CK1d+ in the open field, however females did not show increased mobility in any of the parameters tested after CCI compared to their sham controls including distance travelled time spent in center, and maximal speed (Figure 40).

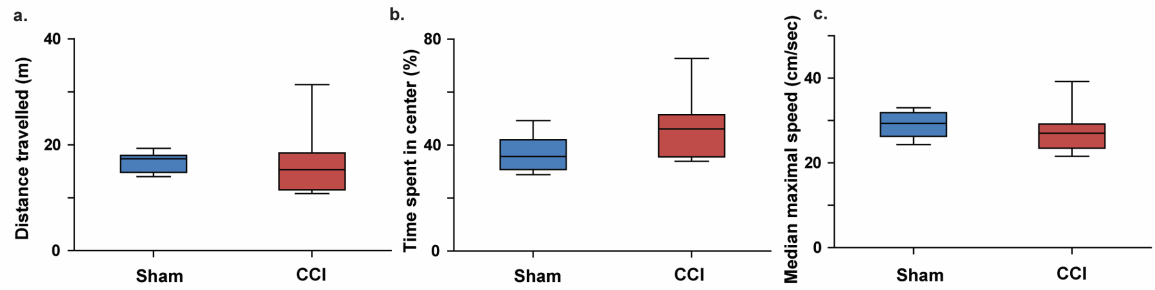

Figure 40: Box whisker plots representing activity in the open field test for CK1d+ females. In all graphs, boxes represent median (75th and 25th percentile), and whiskers represent max and min values per each group. No difference was seen in either distance travelled percent time spent in the center or maximal speed between CCI vs. sham females. (n=9, 10 for sham and CCI groups respectively).

We continued to evaluate signs of anxiety in the elevated plus maze (Figure 41). CK1d+ males or their WT counterparts did not show signs of anxiety after CCI in the elevated plus maze test compared to their sham controls as indicated by their similar time spent in both the open and closed arms. The distance travelled was also similar in this test, although similar trends were

seen for increased locomotion in CK1d+ and decrease locomotion in CK1d- as shown in the open field test, however these were not significant in this test.

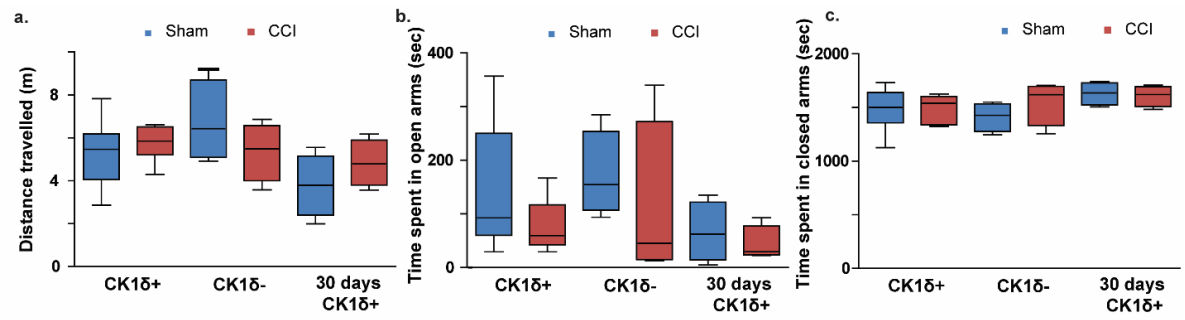

Figure 41: Box whisker plots representing activity in the open field test for CK1d+, CK1d- (WT counterparts) and CK1d+ 30 days, after CCI vs. sham treatment. In all graphs, boxes represent median (75th and 25th percentile), and whiskers represent max and min values per group. **a.** distance travelled. No difference was seen for the distance travelled between CCI and Sham in all groups tested. **b.** time spent in open arms. No difference was seen for the time spent in open arms between CCI and Sham in all groups tested. **c.** Time spent in closed arms. No difference was seen for the time spent in the closed arms between CCI and Sham in all groups tested. (n=7 per group for CK1d+; n=4 per group for CK1d- sham and CCI respectively; n=4 per group for 30 days CK1d+).

However, when we evaluated the anxiety response in female CK1d+, we saw that unlike males, females showed an increased anxiety after CCI compared to Sham controls. Female CK1d+ showed a decrease in distance moved, an increase in time spent in closed arms and a decrease in time spent in open arms. One might suspect that the decrease in distance moved might indicate an immobility effect after CCI which can cause a difference in time spent in the different arms and not anxiety *per se*. However since a day before the test the animals went through the open field test and moved a significantly longer distance, having no difference between sham and CCI in the amount of distance travelled, we suspect that the difference seen in this test is due to anxiety and not an immobility effect.

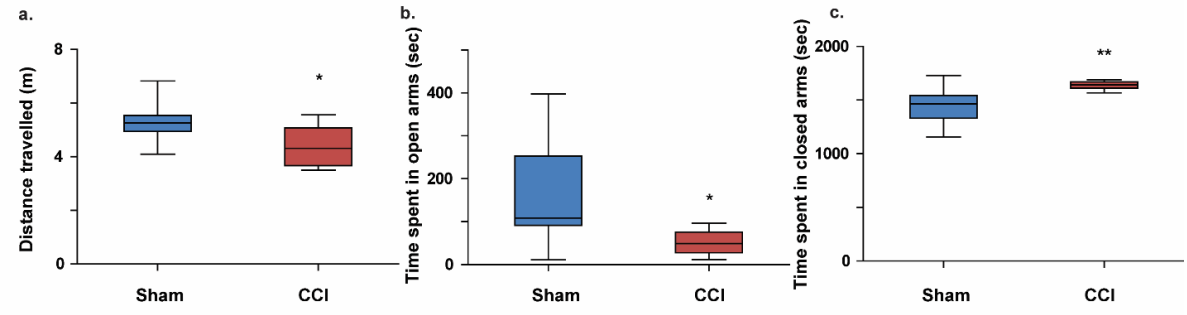

Figure 42: Box whisker plots representing activity in the elevated plus maze test for CK1d+ females. In all graphs, boxes represent median (75th and 25th percentile), and whiskers represent max and min values per each group. **a.** Distance travelled during 30 min of test. CK1d+ females after CCI showed a significant decrease in distance travelled compared to their sham controls. **b.** Time spent in the open arms. CK1d+ females showed a significant decrease in the time spent in the open arms compared to their sham controls. **c.** Time spent in closed arms. CK1d+ females showed an increase in the time spent in closed arms compared to sham controls. These results indicate an increase in anxiety measure for CK1d+

females after CCI compared to sham controls. (*p<0.05, ** p<0.01, Student's t-test, n=9, 10 for sham and CCI groups respectively).

We continued to evaluate mechanical allodynia threshold for CCI vs. sham animals using von-Frey filaments (VFF) 86 hours (four days) after CCI and sham procedure. We also administered nitroglycerine (NTG) which induces a migraine without aura in humans, and reduces hind paw allodynia threshold in rodents, thus serving as a migraine relevant animal model.

We found that both CK1d+ (Figure 43) and CK1d- males (Figure 44) did not show a difference in baseline allodynia after CCI vs. their sham controls. However, CK1d+ males after CCI did not show a typical reduction in mechanical allodynia after administration of NTG (Figure 43b) compared to their sham controls and compared to CK1d- CCI animals (Figure 44), indicating a difference in pain response after NTG for the CK1d+ males after CCI. After 30 days however, CK1d+ males showed a reduced baseline threshold, and a reduction in mechanical allodynia threshold after NTG administration (Figure 45).

When we evaluated female CK1d+ we found that CCI reduced their baseline mechanical allodynia threshold compared to their sham controls and contrary to CK1d+ males (Figure 46). However, after administration of NTG, only the sham controls showed a typical reduction in baseline threshold at both time points after NTG administration, while CCI animals did not show the typical reduction in baseline similar to CK1d+ males.

All groups were also administered with vehicle control and did not show a change in mechanical allodynia in any of the time points evaluated (data not shown).

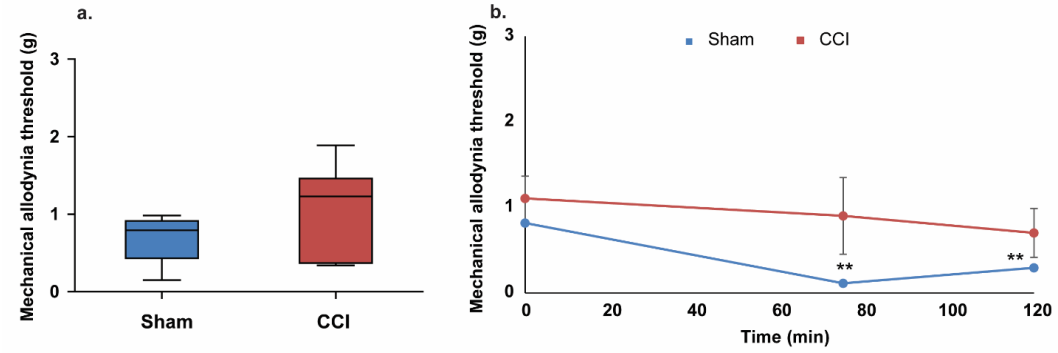

Figure 43: Evaluation of mechanical allodynia after CCI and sham procedures in CK1d+ males. **a.** box whisker plots showing baseline mechanical allodynia threshold for sham vs. CCI CK1d+ males. No difference in baseline threshold was seen between the groups (n=5, 7 for the sham and CCI groups respectively). **b.** mechanical allodynia threshold evaluated at baseline and 75 and 120 min after injection of NTG to both sham and CCI animals. Each point represent mean ± s.e.m. for all animals in the group. Only sham CK1d+ males showed a significant reduction in mechanical allodynia threshold after NTG administration. No difference in mechanical allodynia threshold was seen for the CCI animals after NTG administration (n=3, 4 for the sham and CCI groups respectively).

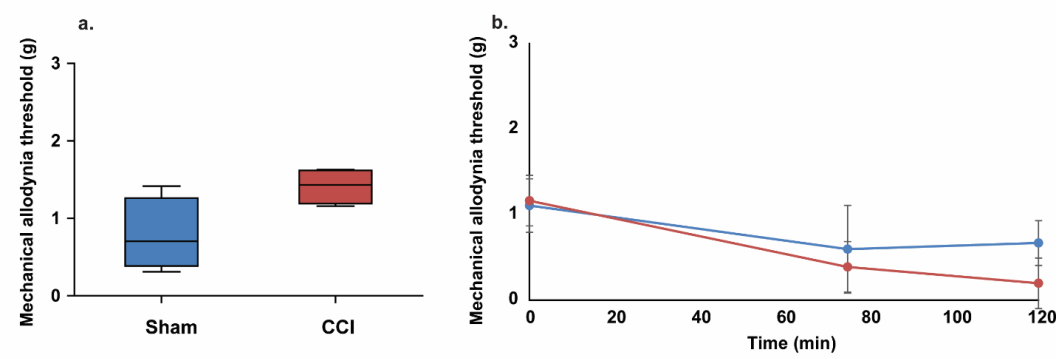

Figure 44: Evaluation of mechanical allodynia after CCI and sham procedures in CK1d- males. **a.** box whisker plots showing baseline mechanical allodynia threshold for sham vs. CCI CK1d- males. No difference in baseline threshold was seen between the groups (n=4 per group). **b.** mechanical allodynia threshold evaluated at baseline and 75 and 120 min after injection of NTG to both sham and CCI animals. Each point represent mean ± s.e.m. for all animals in the group. Both groups showed a reduction in mechanical allodynia threshold after NTG administration (n=2 for the sham and CCI groups respectively).

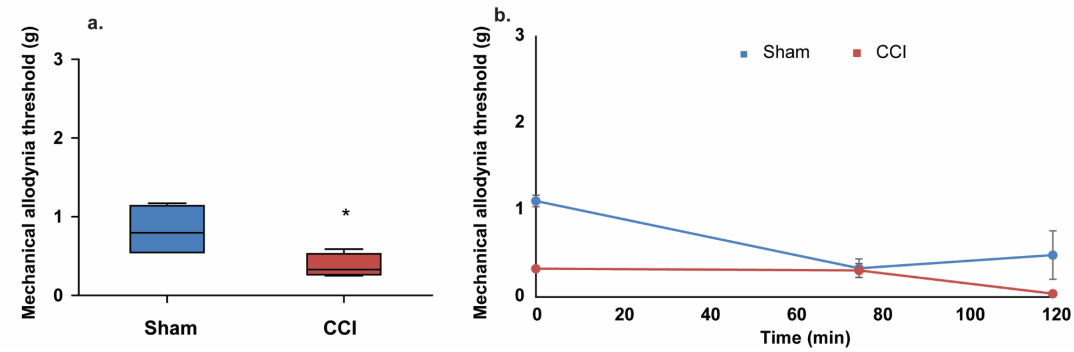

Figure 45: Evaluation of mechanical allodynia after CCI and sham procedures in CK1d+ males 30 days after CCI and sham procedures. **a.** box whisker plots showing baseline mechanical allodynia threshold for sham vs. CCI CK1d+ males. CCI males showed a significant reduction in baseline threshold (n=4 per group). **b.** mechanical allodynia threshold evaluated at baseline and 75 and 120 min after injection of NTG to both sham and CCI animals. Each point represent mean ± s.e.m. for all animals in the group. Sham CK1d+ males showed a reduction in mechanical allodynia threshold after NTG administration. CCI animals showed a reduced threshold after NTG administration only at the 120 min time point (n=2 per group).

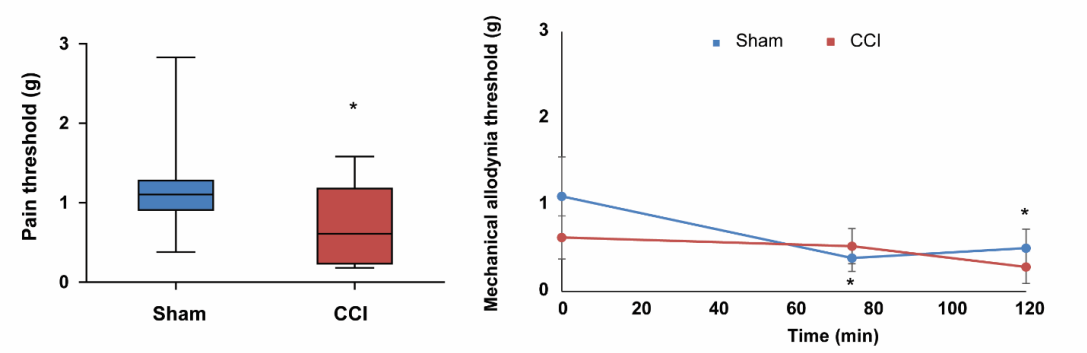

Figure 46: Evaluation of mechanical allodynia after CCI and sham procedures in CK1d+ females. a. box whisker plots showing baseline mechanical allodynia threshold for sham vs. CCI CK1d+ females. Baseline threshold was significantly lower in the CCI group vs. the sham controls (* $p<0.05$, Student's t-test, n=9, 10 for the sham and CCI groups respectively). b. mechanical allodynia threshold evaluated at baseline and 75 and 120 min after injection of NTG to both sham and CCI animals. Each point represent mean ± s.e.m. for all animals in the group. Only the sham group showed a significant reduction in mechanical allodynia threshold after NTG administration. CCI animals did not have a reduced mean mechanical allodynia threshold after NTG administration compared to sham controls (*$p<0.05$, Tukey multiple comparison test, n=5 per group).

We evaluated CSD frequency in male CK1d+, CK1d-, CK1d+ after 30 days, and CK1d+ females. We found that only females showed a significant increase in number of CSDs for the CCI group compared to sham controls, where none of the other groups showed a significant change in CSD frequency between sham and CCI (Figure 47).

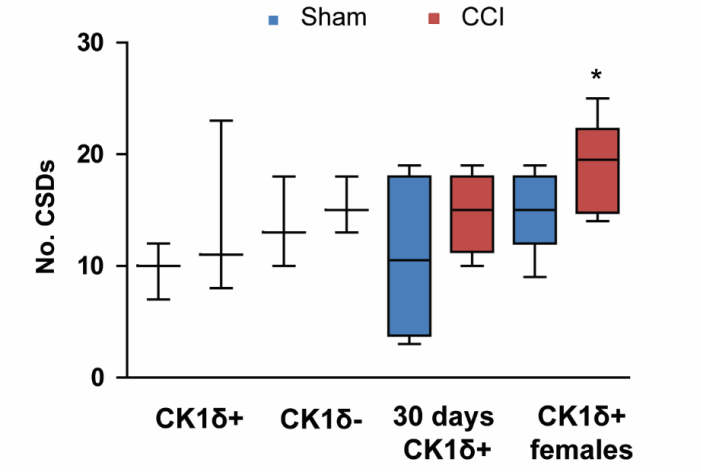

Figure 47: Box whisker plots representing number of CSDs for CK1d+, CK1d- (WT counterparts) and CK1d+ 30 days, and CK1d+ females after CCI vs. sham treatment. Only CK1d+ females showed a significant increase in no. of CSDs after CCI vs. sham control. (*$p<0.05$. student's t-test, n=3 per group for CK1d+ CCI vs. sham; n=3 per group for CK1d- CCI vs. sham; n=4 for CK1d+ 30 days for CCI vs. sham; n=9, 10 for CK1d+ females CCI vs. sham)

Subtask 7. Analyze results, correlate with histological and other experimental data, prepare data for publication.

Reported with each sub-task.

Specific Aim 3:
Test whether medications that modulate post-TBI plasticity reduce markers of epilepsy and migraine after TBI.

Major Task 3:
Chronic experiments after CCI TBI (Brennan, Dudek Months 1-48).

Subtask 1. Perform CCI, implant monitoring device, and monitor for effects of memantine treatment after TBI (3 months after injury).

Please see Specific Aim 1, Subtask 1 above. The rate of seizures was too low for these experiments to have statistical power without a number beyond our capacity – for a power of 80% to detect a difference at alpha of 0.05, we would need 60 animals *per group.* This was well beyond our budgeted animals as well as beyond the throughput of the monitoring racks. However, beyond the scope of this grant, we are continuing this line of inquiry (Co-Investigator Dudek is funded by NIH/DoD for long-term monitoring after brain injury). Moreover, we investigated (see below), and continue to investigate (in PR 130373) the effects of memantine after TBI, in this case with a focus on pain metrics.

Subtask 2. Perform nociception behavior experiments (mechanical and thermal thresholds, rotarod) on animals 3 months after CCI TBI and treatment with memantine or placebo.

Memantine effects on nociception behavior
We evaluated the effect of 14±1 days treatment with 30 mg/kg memantine vs. vehicle, on mechanical allodynia threshold post sham and CCI. Thirty two male C57Bl/6 mice were randomly divided to 4 groups: Sham/vehicle, Sham/memantine, CCI/vehicle and CCI/memantine. All animals had either sham or CCI surgery according to a previously reported method. Prior to the experiment mice were evaluated for their daily water intake to be 200 ml/kg/day for 2% sucrose in drinking water (the vehicle used in the experiment). An hour after the end of either sham or CCI surgery, memantine was dissolved in 2% sucrose in drinking water and was added to both the sham/memantine or CCI/memantine group cages. In order to achieve a daily intake of 30 mg/kg memantine per mouse, all mice had their fluid consumption evaluated daily and the amount of memantine added to the drinking water was adjusted accordingly. A week before commencement of mechanical allodynia testing, mice were handled daily for 2 min using the cupped hand technique in order to avoid the effect of stress on mechanical allodynia threshold during testing. On the test day, mice were allowed to acclimate to the elevated wire mesh floor apparatus (IITC life science, Woodland Hills, CA) for 2 hours. Mechanical alldynia was measured on both hind paws (starting from the left hind paw) using Dixon's up-and-down method as previously published[28]. Mechanical allodynia threshold was determined as the threshold mean for both hind paws. No change in mechanical allodynia was noticed between either of the four groups tested (Figure 48). It is possible that since no reduction in mechanical allodynia was noticed after CCI, memantine could not exert its anti-allodynic effect in this model.

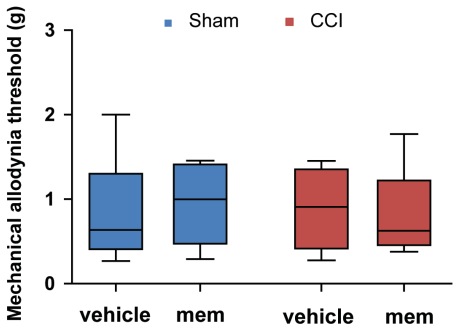

Figure 48: Box whisker plots representing mechanical allodynia threshold in sham and CCI treated with both vehicle and memantine (mem). No significant difference in mechanical allodynia was seen between the groups. (n=9, 8, 8, 7 for the Sham/veh, sham/memantine, CCI/veh and CCI/memantine groups respectively).

Memantine effects on neuronal cell death

Analysis of FJB staining indicated that there was no cell loss/necrosis in the somatosensory cortical region and also in any other regions (e.g., hippocampus, amygdala) at 14 days after CCI in vehicle or memantine treated animals. As expected we did not see any neuronal damage in sham-treated animals.

To determine whether memantine resulted in reduced brain damage, total contusion area was measured in mice on 14 days post-CCI (Figure 49). Histological examination of sections exhibited that CCI injury produced moderate level of focal lesion/damage in the ipsilateral somatosensory cortex at 14 days after injury. Cortex lost its normal conformation at the concussion site, specifically a cavity was observed with irregular edges that did not extend to the subcortical structures mainly hippocampus (Figure 49).

The graph in Figure 49 shows that the area of cortical contusion lesion in the ipsilateral cortex as a percentage of the contralateral uninjured cortex was 2.5% in memantine and CCI group (n = 6 animals), whereas the area of lesion was 2.48 % in the vehicle and CCI group (n = 6 animals) at 14 days post-injury. 1 out 10 sham treated animals showed lesion in the ipsilateral cortical side relative to contralateral. Lesion areas were of comparable size in both treatment groups. Overall, non-significant changes in lesion area was detected (unpaired t-test: $p > 0.05$) in memantine CCI as compared to vehicle CCI group.

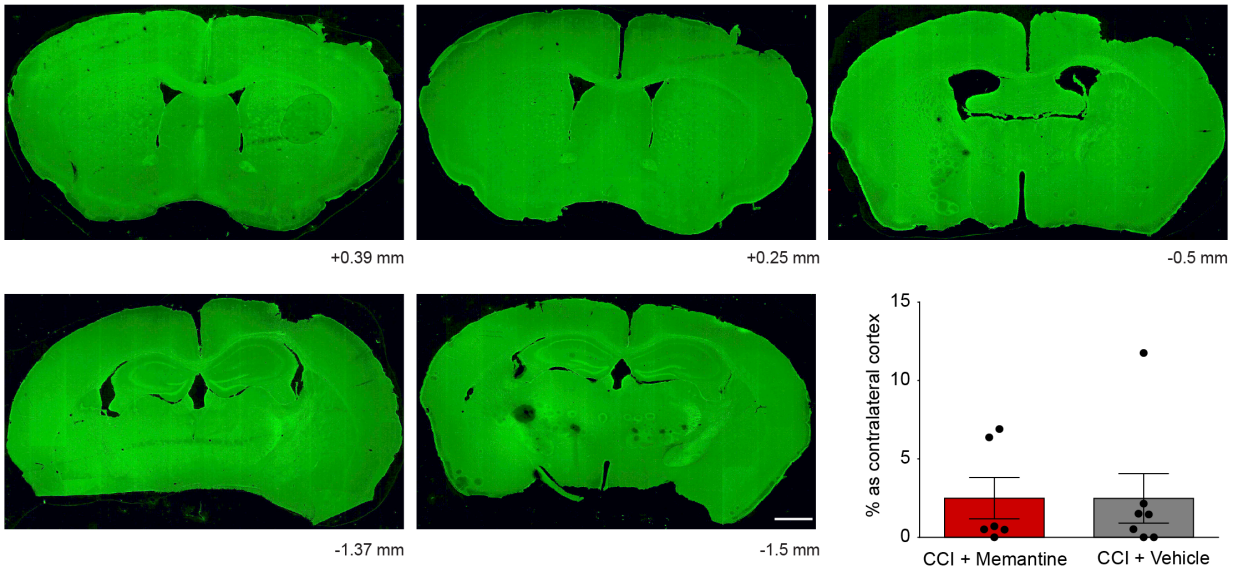

Figure 49: Left: Series of sections showing neurodegeneration in a typical brain of male mice subjected to controlled cortical impact injury (1 mm depth; impactor 1 mm in diameter) at 14 days post-injury. Sections from sham-treated mice (craniotomy but no impact) showing no lesion in the ipsilateral cortex (data not shown). Right: Bar graph shows the area of cortical contusion in the ipsilateral cortex as a percent of the area of the contralateral cortex as measured by Nanozoomer. Data shows average of three sections that showed highest level of lesion. The brains were stained with FluoroJade.

Subtask 3. Analyze results, correlate with histological and other experimental data, prepare data for publication.

Reported with each sub-task.

4. KEY RESEARCH ACCOMPLISHMENTS

Technical/Methodological

•Optimized controlled cortical impact TBI (CCI) parameters for mouse – nearly all work prior to this award had been done in rat. Mouse preparations are key to using genetic indicators and genetic models of disease (see below).

•Optimized EEG monitoring of mice after CCI to monitor for seizures and cortical spreading depression (CSD), continuously out to 90 days after CCI – significant technical advance due to long term and remote telemetric nature of recordings.

•Implemented two-photon microscopy after CCI – this was a major technical hurdle due to the need to adjust craniotomy techniques to allow imaging near an injury area.

•Implemented *in vivo* whole cell recording after CCI – this was a significant technical advance due to the need to record from injured cortex.

•Deployed genetically-encoded calcium indicators after TBI.

•Determined that voltage sensitive dye imaging is not optimal for TBI models due to artifactual binding to injured tissue.

Scientific

•CCI TBI generates seizures consistent with post-traumatic epilepsy – confirmation of key hypothesis of the grant.

•Sham TBI procedures involving craniotomy also generates seizures consistent with post-traumatic epilepsy – potential reportable confound in TBI epilepsy research – evidences a need for a greater range of control conditions including animals with no surgical intervention.

•CCI TBI is universally associated with cortical spreading depression (CSD) – key hypothesis of the grant confirmed – validates the study of CSD and other spreading depolarizations as TBI injury mechanisms.

•CSD alters neuronal excitability for over an hour, with distinct effects on excitatory and inhibitory input – first *in vivo* whole cell recordings of CSD, providing actionable presynaptic and postsynaptic targets for therapeutic intervention.

•Lipopolysaccharide (LPS) injection confers protection from CSD in wild type mice – suggesting that inflammatory mechanisms after TBI may protect from injury associated depolarizations.

•In contrast, LPS injection is *not* protective in mice with a knockout of the astrocytic STAT3 gene, suggesting astrocytic activation as a mechanism of CSD neuroprotection.

•Determined minimum thresholds for induction of CSD, providing quantitative data on tissue injury thresholds relevant to TBI.

•Prodromal activation of astroyctic networks by potassium enables the propagation of CSD – basic cellular mechanism underlying TBI injury mechanism.

•Sensory cortex is more susceptible to CSD and anoxic depolarization in mice and in human – possible explanation of sensory dysfunction including post-traumatic headache after TBI.

•Mice carrying a migraine mutation (casein kinase 1 delta; CK1d) have greater susceptibility to CSD, as well as headache-related pain metrics.

•CCI TBI increases the excitability of individual sensory cortex neurons in wild-type mice – confirmation of key grant hypothesis.

•CCI TBI causes significantly *greater* increases in the neuronal excitability of CK1d migraine mutant mice – first scientific validation of the clinical observation that patients with migraine are more susceptible to post-traumatic headache.

•Increased CSD-associated neuronal calcium load in CK1d animals compared to WT after CCI TBI – consistent with increased excitability and possibly greater CSD-associated damage after TBI.

•CK1d female mice have distinct behavioral responses after TBI compared with both male CK1d mice and wild type mice, showing decreased mechanical pain thresholds and increased anxiety. This is consistent with the clinical observation that females with migraine are most susceptible to PTH.

•In contrast to CK1d male and wild type mice, CK1d female mice have increased susceptibility to CSD after TBI – evidence of sex- and migraine-gene-specific modulation of post-TBI excitability.

•Memantine is protective after ischemic cortical injury – confirmation of key preliminary data for this proposal.

•Memantine data so far inconclusive after CCI, but will be continued in CDMRP PR 130373.

5. CONCLUSION

Our proposal has examined the natural history and mechanisms of increased brain excitability leading to migraine and epilepsy after traumatic brain injury (TBI). In order to pursue our work, we have pioneered or significantly advanced new techniques for the study of TBI, including continuous remote telemetry, *in vivo* whole cell recording, and two-photon imaging with genetically encoded calcium indicators. We have generated multiple reportable outcomes, providing experimental evidence that: 1. TBI causes seizures; 2. TBI increases neuronal excitability, an effect that is enhanced in 'migraine' mutant mice; 3. TBI is universally associated with spreading depolarizations that are also involved in migraine; 4. sensory cortex is more susceptible to spreading depolarizations, consistent with prominent sensory and pain features after TBI; 5. the effects of TBI are amplified by female sex as well as migraine genotype, consistent with what is observed in the clinic. We have published four manuscripts (in Science Translational Medicine, Stroke, Journal of Neurophysiology, and Cephalalgia); two more are pending publication; and four more manuscripts are in preparation. This work also continues in CDMRP PR130373. We are very grateful for the opportunities this award has given us to understand and hopefully better treat the diseases that affect the men and women of our armed forces.

6. PUBLICATIONS, ABSTRACTS, AND PRESENTATIONS

Lay Press

Utah Researchers Investigate Seizures and Migraine After Brain Injury
Study Aims to Improve Outcomes for Soldiers, Others.
http://healthcare.utah.edu/publicaffairs/news/archive/2011/10-12-11_Seizures and Migraine Brain Injury.php.

Healing Hidden Wounds: U of U researchers team up to study military brain injury. Convergence 2012 – *University of Utah Health Care Annual Report to the Community.*

BYU, Utah researchers find genetic cause for migraines. Deseret News, May 1 2013.
http://www.deseretnews.com/article/865579279/BYU-Utah-researchers-find-genetic-cause-for-migraines.html?pg=all

Utah Researchers Make Discovery That Could Help Migraine Patient. KUTV News, May 1 2013.
http://kutv.com/top-stories/stories/vid_4789.shtml

Rabin RC (2014). Health Researchers Will Get $10.1 Million to Counter Gender Bias in Studies. New York Times, September 23, 2014.
http://www.nytimes.com/2014/09/23/health/23gender.html?ref=health&_r=0

Peer-reviewed Publications

1. Brennan KC, Bates EA, Shapiro RE, Zyuzin J, Hallows WC, Huang Y, Lee HY, Jones CR, Fu YH, Charles AC, Ptacek LJ. Casein kinase 1 delta mutations in familial migraine and advanced sleep phase. Sci Transl Med 2013; 5(183):183ra56, 1-11. PMCID: PMC4220792. *Cover; Editorial focus. Also supported by CDMRP PR100054 (A.Charles).*

2. Lopez-Valdes HE, Clarkson AN, Ao Y, Charles AC, Carmichael ST, Sofroniew MV, Brennan KC. Memantine enhances recovery from stroke. Stroke 2014;45(7):2093-100. PMCID: PMC4142682.

3. Tang YT, Mendez JM, Theriot JJ, Sawant PM, Lopez-Valdes HE, Ju YS, Brennan KC. Minimum Conditions for the Induction of Cortical Spreading Depression in Brain Slices. J Neurophysiol 2014;15;112(10):2572-9. PMCID: PMC4233272.

4. Kaufmann D, Bates EA, Yagen B, Bialer M, Saunders GH, Wilcox K, White HS, Brennan KC (2015). *sec*-Butylpropylacetamide (SPD) Has Anti-Migraine Properties. *Cephalalgia, In press.*

Note: CDMRP PR100060 was erroneously not cited as a source of funding for 1 and 2 above. This work was integral to the proposal, and was conducted in part with CDMRP support. With GOR approval, we would like to contact the journals to fix this error, adding a formal Correction to each manuscript.

Invited Reviews

1. Ayata C, Brennan KC. Animal models of migraine aura. In *The Neurological Basis of Migraine.* NY Academy of Sciences/Wiley. *This is a comprehensive review of CSD, which this project has shown is also an integral mechanism of TBI.*

Publications Pending

1. Sawant PM, Suryavanshi P, Mendez JM, Dudek FE, Brennan KC. Mechanisms of neuronal silencing after cortical spreading depression. *In Revision, Cereb Cortex*.

2. Bogdanov VB, Middleton NA, Theriot JJ, Abdullah OM, Hartings JA for the COSBID Investigators, Brennan KC. Susceptibility of primary sensory cortex to spreading depolarizations. *Under review, J Neurosci. Also supported by CDMRP PH/TBI Research Program (J.Hartings).*

Manuscripts in Preparation

1. Lemkuhle M, Suryavanshi P, Sawant PM, Theriot JJ, Brennan KC, Dudek FE. Incidence of seizures and neuronal suppression in 90 day continuous monitoring after traumatic brain injury. *In preparation.*

2. Sawant PM, Suryavanshi P, Rea N, Kilby J, Service CA, Mendez JM, Dudek FE, Brennan KC. Migraine genotype alters the neuronal response to traumatic brain injury. *In final preparation.*

3. Mendez JM, Sawant PM, Theriot JJ, Suryavanshi P, Kaufmann D, Brennan KC. Prodromal events enable the propagation of spreading depolarization. *In final preparation.*

4. Kaufmann D, Rea N, Sawant PM, Theriot JJ, Brennan KC. Migraine genotype and female sex additively increase the response to traumatic brain injury. *In preparation.*

Abstracts (* those with asterisk have resulted in submitted publications)

Tang T, Lopez-Valdes HE, Ju YS, Charles AC, Brennan KC (2012). Minimum conditions for the induction of cortical spreading depression: implications for migraine and brain injury. American Academy of Neurology Annual Meeting, New Orleans LA – Selected for platform Presentation. *

Mendez J, Theriot J, Brennan KC (2013). In vivo cell specific characterization of cortical spreading depression Society for Neuroscience Annual Meeting, San Diego CA. Selected for Dynamic Poster Presentation (Abstract).

Sawant PM., Dudek FE., Brennan KC. *In vivo* whole-cell recording of neocortical neurons during cortical spreading depression. Society for Neuroscience Annual Meeting, San Diego CA. (Abstract).

Bogdanov VB, Brennan KC. (2013). Preference of cortical spreading depression for sensory cortex. . International Headache Congress, Boston MA – Selected for platform presentation (Abstract). *

Mendez JM, Theriot JT, Brennan KC (2014). In vivo cellular dynamics of cortical spreading depression. American Headache Society Annual Meeting, Los Angeles, CA – Selected for platform presentation (Abstract).

Sawant PM, Suryavanshi P, Brennan KC (2014). In vivo single neuron effects of traumatic brain injury on wild type and migraine transgenic mice. American Headache Society Annual Meeting, Los Angeles CA – Selected for platform presentation (Abstract). *

Mendez JM, Sawant PM, Theriot JJ, Suryavanshi P, Brennan KC (2015). Spreading depression at cellular resolution. International Headache Society, Valencia Spain and American Headache Society, Washington DC – Selected for platform presentation (Abstract).

Bogdanov VB, Middleton NA, Theriot JJ, Abdullah OM, Hartings JA for the COSBID Investigators, Brennan KC (2015). Susceptibility of primary sensory cortex to spreading depolarizations. Co-Operative Study on Brain Injury Depolarizations Conference, Helsingor Denmark. Selected for platform presentation (Abstract). *

Parker PD, Theriot JJ, Mendez JM, Brennan KC (2015). Altered sensory processing following cortical spreading depression in awake mice. Society for Neuroscience Annual Meeting, Chicago IL. (Abstract). *

Suryavanshi P, Sawant PM, Brennan KC (2015). Synaptic mechanisms of cortical spreading depression. Society for Neuroscience Annual Meeting, Chicago IL. (Abstract).

Sawant PM, Brennan KC (2015). Intrinsic and synaptic activity of excitatory neurons in layer 2/3 somatosensory cortex of CK1d migraine mice after traumatic brain injury. Society for Neuroscience Annual Meeting, Chicago IL. (Abstract). *

Invited presentations during last year (* those with asterisk have resulted in submitted publications)

Cortical spreading depression and its effects on the sensory brain. University of New Mexico Neuroscience Seminar, 5/8/14.

Does my mouse have a headache? Investigating the basic science of migraine and post-traumatic headache. University of Iowa Neuroscience Seminar, Iowa City, IA, 5/14/14. *

Investigating the sensory dysplasticity of headache. University of California Los Angeles Grand Rounds, 6/25/14. *

Spreading depolarizations of the brain. Penn State Neuroscience Seminar, 3/10/15. *

Spreading depression at cellular resolution. International Headache Congress, Valencia Spain, 5/15/15; American Headache Society Annual Meeting, 6/20/15. *

Susceptibility of primary sensory cortex to spreading depolarizations. Co-Operative Study of Brain Injury Depolarizations Meeting, Helsingor Denmark, 9/10/15. *

7. INVENTIONS, PATENTS, AND LICENSES

None to report.

8. REPORTABLE OUTCOMES

•CCI TBI generates seizures consistent with post-traumatic epilepsy – confirmation of key hypothesis of the grant.
•Sham TBI procedures involving craniotomy also generates seizures consistent with post-traumatic epilepsy – potential reportable confound to TBI epilepsy research – evidences a need for a greater range of control conditions including animals with no surgical intervention.
-These findings are combined in a manuscript currently in preparation (Manuscript in Preparation 1 above). This is the first longitudinal, chronic monitoring that shows generation of seizures after TBI. It is also an important methodological lesson for the research community that our currently accepted sham treatments also generate seizures.

•CCI TBI is universally associated with cortical spreading depression (CSD) – key hypothesis of the grant confirmed – validates the study of CSD and other spreading depolarizations as TBI injury mechanisms.
•CCI TBI increases the excitability of individual sensory cortex neurons in wild-type mice – confirmation of key grant hypothesis.
•CCI TBI causes significantly *greater* increases in the neuronal excitability of CK1d migraine mutant mice – first scientific validation of the clinical observation that patients with migraine are more susceptible to post-traumatic headache.
•Increased CSD-associated neuronal calcium load in CK1d animals compared to WT after CCI TBI – consistent with increased excitability and possibly greater CSD-associated damage after TBI.
-These findings are combined in a manuscript in final stages of preparation (Manuscript in Preparation 2 above). To our knowledge it is the first use of in vivo *whole cell recording after TBI, as well as the first use of an animal migraine model to dissect disease-specific mechanisms after brain injury.*

•CSD alters neuronal excitability for over an hour, with distinct effects on excitatory and inhibitory input – first *in vivo* whole cell recordings of CSD, providing actionable presynaptic and postsynaptic targets for therapeutic intervention.
-Revised manuscript resubmitted to Cerebral Cortex.

•Lipopolysaccharide (LPS) injection confers protection from CSD in wild type mice – suggesting that inflammatory mechanisms after TBI may protect from injury associated depolarizations.
•In contrast, LPS injection is *not* protective in mice with a knockout of the astrocytic STAT3 gene, suggesting astrocytic activation as a mechanism of CSD neuroprotection.
-These results are reportable combined; however we would like to expand our histological analysis of this dataset before submitting.

•Determined minimum thresholds for induction of CSD, providing quantitative data on tissue injury thresholds relevant to TBI.
-Published (Peer-reviewed Publications 3).

•Prodromal activation of astroyctic networks by potassium enables the propagation of CSD – basic cellular mechanism underlying TBI injury mechanism.
-Manuscript in final stages of preparation (Manuscript in preparation 3 above). To our knowledge this is the first combined two-photon microscopy/ in vivo *whole cell investigation of CSD.*

•Sensory cortex is more susceptible to CSD and anoxic depolarization in mice and in human – possible explanation of sensory dysfunction including post-traumatic headache after TBI.
-Under review at the Journal of Neuroscience (Publications Pending 2). This work in both animals and humans (in collaboration with Dr. Jed Hartings and additionally supported by the CDMRP PH/TBI Research Program is the first to systematically examine the susceptibility of different brain regions to the spreading depolarizations associated with TBI.

•Mice carrying a migraine mutation (casein kinase 1 delta; CK1d) have greater susceptibility to CSD, as well as headache-related pain metrics.
-Published (Peer-reviewed Publication1). This work was on the cover of Science Translational Medicine, with an Editorial Highlight. It was also supported by another CDMRP grant, PR 100054, to Dr. Andrew Charles. The CK1d 'migraine' mouse has allowed us to significantly increase the mechanistic precision and headache relevance of our investigations. We continue to use this mouse in CDMRP PR 130373.

•CK1d female mice have distinct behavioral responses after TBI compared with both male CK1d mice and wild type mice, showing decreased mechanical pain thresholds and increased anxiety. This is consistent with the clinical observation that females with migraine are most susceptible to PTH.
•In contrast to CK1d male and wild type mice, CK1d female mice have increased susceptibility to CSD after TBI – evidence of sex- and migraine-gene-specific modulation of post-TBI excitability.
-These findings are combined in a manuscript in of preparation (Manuscript in Preparation 4) – we need to increase the number of selected experiments to be ready to submit.

9. OTHER ACHIEVEMENTS

This work has supported the graduate training of Tanye Tang, PhD, and Pratyush Suryavanshi, PhD Candidate. It has supported the postgraduate training of Drs. Jorge Mendez, Punam Sawant, and Jay Vargas.

10. REFERENCES

1. Bruns J, Hauser WA. The Epidemiology of Traumatic Brain Injury: A Review. Epilepsia 2003;44(s10):2–10.[cited 2010 Aug 1]

2. Ghajar J. Traumatic brain injury. Lancet 2000;356(9233):923–929.[cited 2010 Aug 1]

3. Rogawski MA. Common pathophysiologic mechanisms in migraine and epilepsy. Arch. Neurol. 2008;65(6):709–714.[cited 2010 Mar 9]

4. D'Ambrosio R, Fairbanks JP, Fender JS, et al. Post-traumatic epilepsy following fluid percussion injury in the rat. Brain J. Neurol. 2004;127(Pt 2):304–314.[cited 2010 Aug 1]

5. Cole JT, Yarnell A, Kean WS, et al. Craniotomy: true sham for traumatic brain injury, or a sham of a sham? J. Neurotrauma 2011;28(3):359–369.

6. Brody DL, Mac Donald C, Kessens CC, et al. Electromagnetic controlled cortical impact device for precise, graded experimental traumatic brain injury. J. Neurotrauma 2007;24(4):657–673.[cited 2010 Aug 1]

7. Brennan KC, Romero Reyes M, Lopez-Valdes HE, et al. Reduced threshold for cortical spreading depression in female mice. Ann Neurol 2007;61(6):603–6.

8. Brennan KC, Beltrán-Parrazal L, López-Valdés HE, et al. Distinct vascular conduction with cortical spreading depression. J. Neurophysiol. 2007;97(6):4143–4151.

9. Brennan KC, Bates EA, Shapiro RE, et al. Casein kinase iδ mutations in familial migraine and advanced sleep phase. Sci. Transl. Med. 2013;5(183):183ra56, 1–11.

10. Somjen GG. Mechanisms of spreading depression and hypoxic spreading depression-like depolarization. Physiol Rev 2001;81(3):1065–96.

11. Herrmann JE, Imura T, Song B, et al. STAT3 is a critical regulator of astrogliosis and scar formation after spinal cord injury. J. Neurosci. Off. J. Soc. Neurosci. 2008;28(28):7231–7243.[cited 2011 Jan 11]

12. Aaronson DS, Horvath CM. A road map for those who don't know JAK-STAT. Science 2002;296(5573):1653–1655.[cited 2012 Sep 8]

13. Oliva AA Jr, Kang Y, Sanchez-Molano J, et al. STAT3 signaling after traumatic brain injury. J. Neurochem. 2012;120(5):710–720.[cited 2012 Sep 8]

14. Tang YT, Mendez JM, Theriot JJ, et al. Minimum conditions for the induction of cortical spreading depression in brain slices. J. Neurophysiol. 2014;112(10):2572–2579.

15. Stosiek C, Garaschuk O, Holthoff K, Konnerth A. In vivo two-photon calcium imaging of neuronal networks. PNAS 2003;100(12):7319–7324.

16. Tian L, Hires SA, Mao T, et al. Imaging neural activity in worms, flies and mice with improved GCaMP calcium indicators. Nat Meth 2009;6(12):875–881.[cited 2011 Oct 17]

17. Zariwala HA, Borghuis BG, Hoogland TM, et al. A Cre-Dependent GCaMP3 Reporter Mouse for Neuronal Imaging In Vivo. J. Neurosci. 2012;32(9):3131–3141.[cited 2012 Sep 27]

18. Shigetomi E, Bushong EA, Haustein MD, et al. Imaging calcium microdomains within entire astrocyte territories and endfeet with GCaMPs expressed using adeno-associated viruses. J. Gen. Physiol. 2013;141(5):633–647.

19. Marvin JS, Borghuis BG, Tian L, et al. An optimized fluorescent probe for visualizing glutamate neurotransmission. Nat. Methods 2013;10(2):162–170.

20. Lucas S, Hoffman JM, Bell KR, et al. Characterization of headache after traumatic brain injury. Cephalalgia Int. J. Headache 2012;32(8):600–606.[cited 2012 Sep 7]

21. Margrie T, Brecht M, Sakmann B. In vivo, low-resistance, whole-cell recordings from neurons in the anaesthetized and awake mammalian brain. Pflüg. Arch. Eur. J. Physiol. 2002;444(4):491–498.[cited 2012 Oct 30]

22. Isaacson JS, Scanziani M. How inhibition shapes cortical activity. Neuron 2011;72(2):231–243.

23. Brennan KC, Charles A. An update on the blood vessel in migraine. Curr. Opin. Neurol. 2010;23(3):266–274.[cited 2012 Feb 25]

24. Meeks JP, Mennerick S. Astrocyte membrane responses and potassium accumulation during neuronal activity. Hippocampus 2007;17(11):1100–1108.

25. Zhou M, Xu G, Xie M, et al. TWIK-1 and TREK-1 are potassium channels contributing significantly to astrocyte passive conductance in rat hippocampal slices. J. Neurosci. Off. J. Soc. Neurosci. 2009;29(26):8551–8564.

26. Hwang EM, Kim E, Yarishkin O, et al. A disulphide-linked heterodimer of TWIK-1 and TREK-1 mediates passive conductance in astrocytes. Nat. Commun. 2014;5:3227.

27. Theriot JJ, Toga AW, Prakash N, et al. Cortical sensory plasticity in a model of migraine with aura. J Neurosci 2012;32(44):15252–61.

28. Chaplan SR, Bach FW, Pogrel JW, et al. Quantitative assessment of tactile allodynia in the rat paw. J. Neurosci. Methods 1994;53(1):55–63.

11. APPENDICES

None.